CHARACTERIZING A NEW REGULATOR OF THE ATR SIGNALING PATHWAY

by

Megan Dalia Biller

A thesis submitted to the faculty of
The University of North Carolina at Charlotte
in partial fulfillment of the requirements
for the degree of Master of Science in
Biology

Charlotte

2022

Approved by:

Dr. Junya Tomida

Dr. Kausik Chakrabarti

Dr. Shan Yan

ABSTRACT

MEGAN DALIA BILLER. Characterizing a New Regulator of the ATR Signaling Pathway.
(Under the direction of DR. JUNYA TOMIDA)

Cellular responses to DNA damage and replication stress are coordinated by an intricate network of repair pathways known as the DNA damage response (DDR). Central to the DDR is the essential kinase ataxia telangiectasia mutated and Rad3-related (ATR**)**, along with its indispensable subunit ATR-interacting protein (ATRIP). Following recruitment and activation, ATR phosphorylates a number of effector proteins, including p53 and CHK1, to initiate DNA repair, cell cycle checkpoints, and replication fork stability. Failure to properly activate such pathways can lead to genome instability, cell death, and development of diseases including cancer. However, the ATR signaling pathway has not yet been established. An incomplete understanding of DDR regulatory mechanisms hinders our ability to effectively diagnose and treat a range of diseases, especially since ATR inhibitors have emerged as promising cancer therapeutics. Here, we found a novel ATRIP binding partner (ABP) which directly binds to ATRIP, and we identified the interaction site in ATRIP. Genetic knockout of *ABP* in human cells influences the ATR signaling pathway with hydroxyurea and mitomycin C treatment. *In vitro* ATR and ataxia telangiectasia mutated (ATM) kinase assays show that ABP affects phosphorylation signal in ATR/ATM substrates. Overall, this work begins to define a new regulator of the ATR pathway and sheds light on the synergy between various components of the DDR.

ACKNOWLEDGMENTS

First and foremost, I would like to thank my mentor Dr. Junya Tomida. Thank you for trusting me to work alongside you and for enthusiastically guiding me from the moment I started in your lab. Thank you for teaching me your 'crazy' scientist ways, for helping me whenever I needed it (which was a lot), and for pushing me to reach my potential. I truly could not have dreamed of a better mentor and I will be forever grateful for the time I spent learning from you. I would also like to thank my committee members, Dr. Kausik Chakrabarti and Dr. Shan Yan. Thank you both for your valuable input on my project and for expanding my knowledge of science through your classes. To all former and current members of the Tomida lab and others I have worked with over the years, thank you for the companionship and for helping me throughout this journey. Thank you to UNCC for funding my time here through assistantships. Last but not least, I would like to thank my family for always supporting me. You all mean the world to me and I wouldn't be in this position without you.

TABLE OF CONTENTS

LIST OF FIGURES

LIST OF ABBREVIATIONS

53BP1	p53 binding protein 1
9-1-1 complex	RAD9, RAD1, HUS1
ATM	Ataxia telangiectasia mutated
ATR	Ataxia telangiectasia-mutated and Rad3-related
ATRi	ATR inhibitor
ATRIP	ATR-interacting protein
ATRIP 2P/A	ATRIP P235A P240A
CHK1	Checkpoint kinase 1
DDR	DNA damage response
DSB	Double strand break
dsDNA	Double stranded DNA
ETAA1	Ewings tumor-associated antigen 1
HR	Homologous recombination
HU	Hydoxyurea
KD	Kinase dead
MMC	Mitomycin C
NBS1	Nijmegen breakage syndrome protein 1
NHEJ	Non-homologous end joining
p-CHK1	Phosphorylated CHK1
PCNA	Proliferating cell nuclear antigen
Pol	Polymerase
p-p53	Phosphorylated p53
RBM	REV7 binding motif
RPA	Replication protein A
SSB	Single strand break

ssDNA	Single stranded DNA
TopBP1	DNA Topoisomerase II Binding Protein 1
WT	Wild type

CHAPTER 1: INTRODUCTION

1.1 ATR in the DNA damage response

Our genome is continuously exposed to exogenous and endogenous sources of DNA damage which result in thousands of DNA lesions each day [1]. If left unrepaired, DNA damage could lead to mutations that threaten the integrity of the genome and lead to diseases like cancer. In order to mitigate the detrimental effects of DNA damage and to preserve genome integrity, cells have developed an extensive signaling and repair pathway known as the DNA damage response (DDR).

The DDR consists of multiple pathways that regulate DNA repair, DNA replication, and cell cycle progression. Key mediators of the DDR include members of the phosphoinositide 3-kinase related kinase (PIKK) family such as ataxia-telangiectasia mutated (ATM), ATM and Rad3-related (ATR), and DNA dependent protein kinase catalytic subunit (DNA-PKcs). These proteins are serine/threonine kinases which recognize S/TQ motifs on their substrates [2]. Members of the PIKK family contain three conserved domains: FAT, FATC, and PRD [3]. FAT domains are thought to be important in cell transport. The small FATC domain is located on the C-terminal and is necessary for kinase activity. The PRD is the PIKK regulatory domain positioned between the FAT and FATC domains and enhances kinase activity [4]. All three of these domains are thought to be important for protein-protein interactions [3]. While ATM and DNA-PKcs primarily respond to DSBs, ATR can be activated by a wider range of genotoxic stress including DSBs, single stranded breaks (SSBs), and replication stress [5]. The versatility of ATR and its critical role in maintaining genome integrity during DNA replication makes it indispensable for cell viability as its knockout in mice results in embryonic lethality [6] .

Due to its essential nature and its involvement in multiple repair pathways, ATR has become a target for many anti-cancer therapeutics. Not only is ATR involved in DSB repair, but it is also heavily involved in managing replication stress which is directly implicated in oncogenesis [7]. ATR inhibitors (ATRis) have become a recent focus of cancer therapies and there are currently four undergoing clinical trials [8]. Many cancerous cells are known to be deficient in one or more DNA repair pathways. For example, more than 50% of cancers have a deficiency in ATM or p53 [8]. Because of this characteristic, cancer cells rely more heavily on the ATR pathway in order to proliferate and survive. It has been shown that the inhibition of ATR in cancer cells results in cell death, while healthy cells are able to overcome this inhibition by upregulating another repair pathway [8-10]. Additionally, coupling ATRis with other forms of chemotherapy, like cisplatin or irradiation, has shown to result in increased sensitivity and lethality of cancer cells [8].

Given the vital role of ATR in cell survival and its rising clinical importance in cancer therapeutics, it is imperative that we continue to study the ATR pathway and fully understand the mechanisms behind its regulation. The research conducted in this project provides novel insights into ATR regulation by the characterization of a new interacting partner.

1.2 ATR recruitment and activation

ATR activation is a multistep process which consists of ATR recruitment to sites of damage and localization of one or more activators. The key DNA structure required for ATR activation is single stranded DNA (ssDNA) coated by replication protein A (RPA) [11]. ssDNA is formed after many types of DNA damage. DNA lesions encountered during replication can stall polymerases at the replication fork, resulting in stretches of exposed ssDNA. In addition,

DSB end resection can result in ssDNA overhangs. In order to protect ssDNA from nuclease degradation, it is quickly bound by RPA [12]. RPA-ssDNA results in the localization of ATR through its obligate subunit ATRIP, which directly binds to RPA and anchors the ATR-ATRIP complex [11].

Independently of ATR localization, activation requires the presence of an activator. There are currently three known ATR activators: TopBP1, ETAA1, and NBS1. TopBP1 is the main activator of ATR. It is directly recruited to sites of damage and requires additional factors including the Rad17- replication factor C (RFC) complex and the Rad9- Rad1- Hus1 (9-1-1) complex. The order of TopBP1 and complex localization remains controversial. In one model, TopBP1 recruits the Rad17-RFC and 9-1-1 complexes, and Rad17-RFC loads the 9-1-1 complex onto ss-dsDNA junctions [13]. Other evidence indicates that the 9-1-1 complex and Rad17-RFC localize prior to TopBP1, and the loading of the 9-1-1 complex triggers localization of TopBP1[14]. Once localized, TopBP1 directly binds Rad9, ATR, and ATRIP, which results in ATR activation [15]. ETAA1 acts independently of TopBP1 and is recruited to sites of DNA damage by RPA-ssDNA where it binds RPA through two domains. It then directly binds and activates ATR [16, 17]. NBS1 has also been shown to directly bind and activate ATR, however, it does not contain an ATR activation domain (AAD) similar to TopBP1 or ETAA1 and the mechanisms behind its recruitment are still under study [18].

Once activated, ATR initiates an extensive signaling cascade and proteomic analyses have identified hundreds of ATR substrates [19]. At the core of ATR signaling lie two important substrates: CHK1 and p53. Both CHK1 and p53 play significant roles in DNA repair and cell cycle progression. CHK1 is responsible for initiating the G2 checkpoint which ensures efficient duplication of the genome before entering mitosis. During S phase, it can inhibit origin firing and

slow down replication, giving damaged DNA enough time to be repaired [20]. p53 plays an extensive role in DNA repair and is often referred to as the "guardian of the genome" [21]. It is responsible for initiating the G1 checkpoint which is critical to preventing the spread of mutated DNA. If DNA is damaged beyond repair, p53 will signal for the cell to undergo apoptosis, further securing integrity of the genome [22]. ATR mainly phosphorylates CHK1 on serine 345 and p53 on serine 15 [23, 24].

1.3 REV7

REV7 is a versatile protein known to function in many cellular processes including translesion synthesis (TLS), mitotic progression, and regulation of DSB repair pathways (Fig. 2) [25-28] . REV7 is a HORMA domain protein that exists in two conformations, an "open" inactive form, and "closed" active form. Typically, REV7 interacts with its binding partners through a conserved safety belt mechanism in which its C-terminal "safety belt" region wraps around and binds its substrates [29]. The REV7 binding motif (RBM) is highly conserved and consists of φφxPxxxpP (Fig. 5) [30]. φ is an aliphatic amino acid, P is a highly conserved proline, and p is a less conserved proline. REV7 can also form hetero- and homodimers which have been shown to facilitate safety belt closure, although the exact role of dimerization seems to vary depending on the substrate and its importance is still being studied [31, 32]. For example, REV7 dimerization is necessary for its function in the TLS pathway and for binding to SHLD2 in the Shieldin complex [31]. However, the REV7 dimerization mutant R124A is still capable of binding SHLD3 and other peptides [33, 34]. It is thought that REV7 dimerization may expose additional protein binding surfaces or stabilize seatbelt interactions.

REV7's most studied function is in polymerase zeta (pol ζ). Pol ζ consists of a catalytic subunit REV3L (also known as REV3) and a regulatory subunit made up of a REV7 dimer [35]. DNA lesions that have not properly been removed can stall replication machinery leading to further cellular damage. In order for replication to progress, DNA lesions must be bypassed. One means of lesion bypass includes the TLS pathway in which specialized DNA polymerases, including pol ζ, are recruited to replicate past lesions that would otherwise stall normal replicative polymerases. In this model, the stalling of replicative polymerase delta (pol δ) induces monoubiquitination of PCNA by RAD18, which recruits TLS components including REV1 and pol ζ. REV1 binds ubiquinated PCNA and directly interacts with REV7 [36]. Additionally, the accessory subunits of pol δ, POLD2 and POLD3, interact with REV3 [37]. Following these interactions, REV1 facilitates a polymerase switch from pol δ to pol ζ, allowing efficient bypass and extension of the lesion [38, 39].

More recently, REV7 has been identified as a member of the Shieldin complex along with SHLD1, SHLD2, and SHLD3 [40, 41]. In this capacity, REV7 plays an important role in DSB repair pathway choice. Briefly, REV7 and other Shieldin components are recruited to sites of DNA damage in a 53BP1-RIF1 dependent manner [42]. The Shieldin complex, specifically SHLD2, directly binds ssDNA to inhibit end-resection, thus promoting NHEJ over HR [28].

In this work, we reveal a novel interaction between REV7 and the ATR-ATRIP complex, and begin to characterize a new role of REV7 in the DDR.

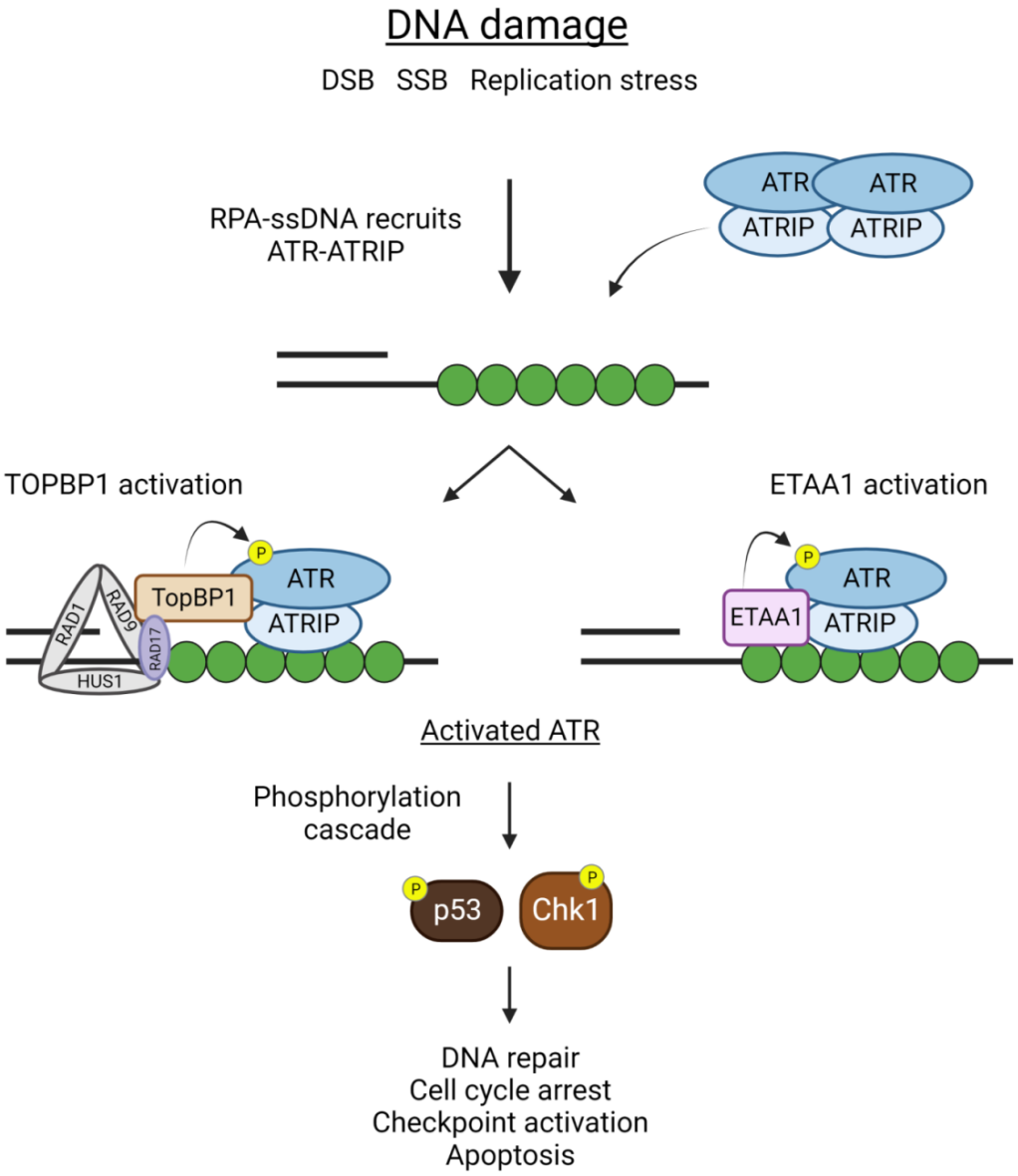

Figure 1. Basic schematic of the ATR pathway.
Many types of DNA damage including double stranded breaks (DSB), single stranded breaks (SSB), and replication stress, result in stretches of exposed single stranded DNA (ssDNA). RPA quickly coats ssDNA which directly recruits the ATR-ATRIP complex. ATR activators TopBP1 and ETAA1 are independently recruited along with accessory factors. Activated ATR initiates a signaling cascade, which includes two main substrates p53 and CHK1.

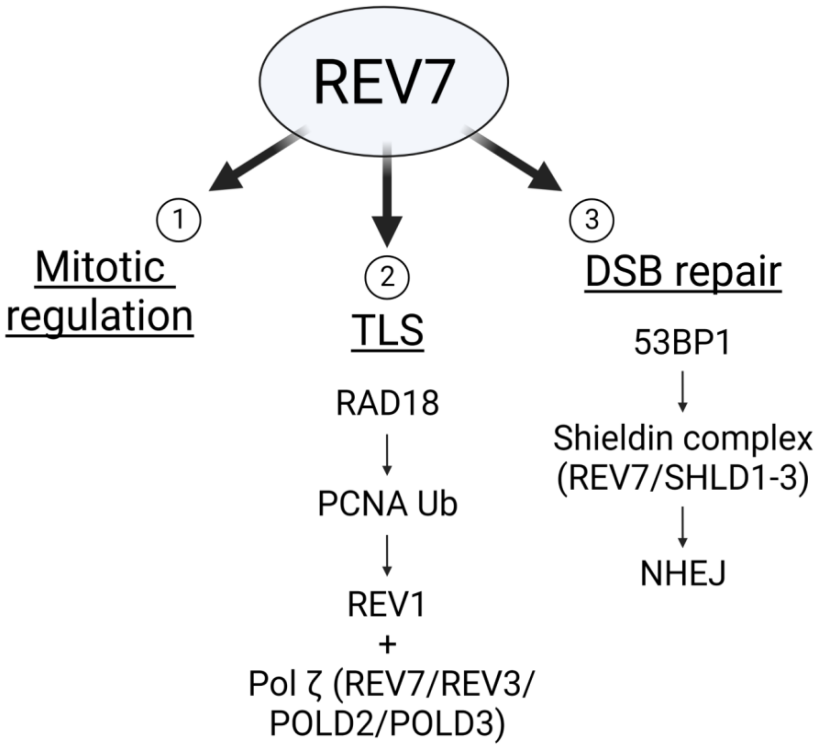

Figure 2. Roles of REV7.
Known roles of REV7 include mitotic regulation, TLS, and DSB repair. 2) REV7 is a component of pol ζ along with REV3, POLD2, and POLD3. Upstream factors include RAD18 which ubiquinates PCNA. REV1 directly interacts with Ub-PCNA and pol ζ to initiate polymerase switching. 3) REV7 is involved in NHEJ DSB repair through the 53BP1 pathway which recruits the Shieldin complex (SHLD3-REV7-SHLD2-SHLD1) to inhibit long range end resection and HR.with accessory factors. Activated ATR initiates a signaling cascade, which includes two main substrates p53 and CHK1.

CHAPTER 2: DEFINING A NEW ROLE OF REV7 IN THE DNA DAMAGE RESPONSE

2.1 Results

REV7 interacts with the ATR-ATRIP complex

Our previous report indicated that REV7 associates with FAM35A [41]. REV7-associated proteins were identified in LC-MS/MS mass spectrometry analysis previously carried out by Tomida et al [41]. In the same set of mass spectrometric data, we also identified the presence of the ATR-ATRIP complex (Fig. 3).

REV7 directly binds to ATRIP P235 P240

To first verify the interaction between REV7 and ATRIP, we performed immunoprecipitation in 293T cells using ATRIP-FH and FH-ATRIP. Endogenous REV7 immunoprecipitated with both N- and C-terminally tagged ATRIP (Fig. 4). Since the RBM is highly conserved across species as PxxxxP, we examined the amino acid sequence of ATRIP which revealed multiple potential RBMs (Fig. 5). Using this information, we then created 4 fragments of ATRIP, each containing an RBM, and cloned them into N-terminally GST-tagged constructs. Each fragment was purified and subjected to a GST pulldown assay with purified His-REV7. Only one fragment showed consistent binding to REV7, ATRIP 203-348, which harbors an RBM at amino acids 232-240 (Fig. 5).

Previous studies have shown that mutating the two conserved prolines in the RBM abolishes the interaction between REV7 and its binding partners [30]. To determine whether ATRIP is indeed a REV7 binding partner and that REV7 binds to the RBM at amino acids 232-340, we created a site directed mutant version of ATRIP 203-348, converting the two conserved

prolines in the RBM to alanine (P235A, P240A: referred to as 2P/A). Significantly, western blot results showed the 203-348 2P/A mutation completely abrogated its interaction with REV7 (Fig. 6).

To further explore the possibility that ATRIP contains more than one REV7 binding region, we next created a full-length version of this mutant, ATRIP FL 2P/A. Surprisingly, the interaction between REV7 and ATRIP FL 2P/A was greatly reduced but not eliminated, suggesting the presence of an additional REV7 binding domain outside amino acids 203-348 (Fig. 6). Given that ATRIP fragments 1-107, 349-507, and 508-791 did not exhibit binding to REV7, we suspected the residual binding between REV7 and ATRIP FL 2P/A may be due to ATRIP's coiled coil region spanning amino acids 108-217. Thus, we purified GST-ATRIP 108-348 2P/A. Pulldown results were consistent with that of ATRIP FL 2P/A, showing a slight interaction with REV7 (Fig. 6). This suggests ATRIP's coiled coil domain may harbor an additional REV7 binding region.

In order to gain further understanding of the interaction between REV7 and ATRIP *in vivo*, we performed IP using ATRIP FL-FH and ATRIP FL 2P/A-FH in 293T cells. Interestingly, endogenous REV7 immunoprecipitated with ATRIP FL, but not ATRIP 2P/A (Fig. 7). This observation may be a product of other factors in the cell which tightly regulate REV7-ATRIP binding. Taken together, these data suggest ATRIP binds REV7 through its RBM at P235 P240, and may also contain an additional REV7 interacting domain in its coiled coil region.

REV7 interaction with ATR

We next sought to explore the interaction between REV7 and ATR. To confirm the mass spectrometry data in figure 3, we expressed FH-ATR in 293T cells and used immunoprecipitates

in a His pulldown assay with purified His-REV7. As expected, His-REV7 was able to pull down ATR (Fig. 9). However, since immunoprecipitates were used and ATR exists naturally bound to ATRIP, this interaction may have been facilitated by ATRIP. To determine whether REV7 directly interacts with ATR, we created 5 GST tagged fragments that each contained an RBM as we previously did with ATRIP (Fig. 10A). We were unable to purify two of these fragments (ATR 1100-1120 and 1120-1230); however, given that the RBMs in these fragments lack the second conserved proline, we do not suspect they directly bind to REV7. Pulldown results from ATR 400-450, 1855-1900, and 1974-2000 did not show a direct interaction with REV7 (Fig. 10B).

Biological effects of REV7 knockout on ATR activity

In order to define the biological importance of REV7's interaction with the ATR-ATRIP complex, we generated *REV7* knockouts (KO) in the TK6 cell line using CRISPR-Cas9 mediated gene editing (Supplementary Fig. 2). We successfully isolated two clones (referred to as MB86 and MB92), and confirmed KO of *REV7* via western blot and PCR (data not shown).

In TK6 WT and *REV7* KO cells, we measured ATR activity through phosphorylation of p53 S15 and CHK1 S345 following treatment with control, MMC, or HU. Compared to WT cells, *REV7* KOs displayed a sharp increase in p53 S15 phosphorylation following treatment with either MMC or HU (Fig. 11). Additionally, phosphorylation of CHK1 S345 was greatly enhanced after treatment with MMC (Fig. 11).

MMC damages DNA through inducing crosslinks while HU stalls replication by depleting deoxynucleotide triphosphates (dNTPs). If not properly repaired, these types of damage can also lead to the formation of DSBs. Since REV7 has known functions in both TLS

(which is required for crosslink repair) and DSB repair, we aimed to identify whether the phenotypes seen in our *REV7* KO lines were due to its known roles in TLS and DSB repair, or an additional function in the ATR pathway. First, to rule out the possibility of impaired TLS resulting in the above phenotypic differences, we examined ATR activity in *REV1*, *REV3,* and *RAD18* KO cells (Fig. 12 A-C). Each of these knockout cell lines displayed increased p-p53 S15 following MMC treatment. In addition, *REV3* KOs showed increased p-p53 following HU treatment (Fig. 12B). Since these phenotypes were also observed in our *REV7* KOs, it is likely a product of hindered TLS. Next, we looked at ATR activity in *53BP1* KO cells when treated with the same DNA damaging agents (Fig. 12D). As a member of the Shieldin complex, REV7 works to inhibit excessive end resection and promote NHEJ following DSBs. This role of REV7 is mediated by 53BP1 which recruits components necessary for NHEJ, including REV7. *53BP1* KOs did not show increased ATR activity via p-p53 or p-CHK1 following DNA damage (Fig. 12D). These results display a unique phenotype of *REV7* KO cells in which MMC induces significant ATR activation, measured by increased p-CHK1 S345. As such, REV7 likely possesses an additional function in the DDR outside its known roles in the Shieldin complex and TLS pathway.

REV7 inhibits ATR activity in vitro

In vivo analysis of ATR activity in *REV7* KO cells raises the overarching possibility that REV7 may be working negatively regulate ATR signaling. In order to assess the direct effect of varying REV7 levels on ATR activity, we performed *in vitro* kinase assays. Flag tagged ATR was transfected into 293T cells, immunoprecipitated, and added to a reaction buffer containing either purified GST-p53 or MBP-CHK1(333-365)-His as a substrate. ATR kinase activity was

monitored by phosphorylation of recombinant p53 at S15 or CHK1 at S345. The immunoprecipitate strongly phosphorylated p53 S15 and CHK1 S345 compared to empty vector control, demonstrating a successful *in vitro* model (Fig. 13A). We then performed additional kinase assays with the addition of purified His-REV7. Significantly, results showed phosphorylation of both p53 S15 and CHK1 S345 decreased in response to increasing amounts of REV7 (Fig. 13 B and C). These observations further support our hypothesis that REV7 functions to attenuate ATR kinase activity.

REV7 directly interacts with p53

The ability of REV7 to decrease ATR activity in our kinase assays could be due to the direct binding of REV7 and ATRIP. Alternatively, REV7 may directly bind substrates and block phosphorylation by ATR. To distinguish between these possibilities, we purified GST tagged p53 and performed a pulldown assay with His-REV7. Surprisingly, results showed a direct interaction between REV7 and p53 (Fig. 14). This suggests two possible mechanisms of REV7 regulation of ATR: directly binding to ATRIP and directly binding to substrates.

Effects of REV7 on ATM kinase activity in vitro

Although mass spectrometry did not detect ATM in the REV7 complex, much of the ATR pathway overlaps with that of ATM. Additionally, ATM and ATR share the ability to phosphorylate many of the same substrates, including p53 on S15. We therefore asked whether REV7 is also capable of inhibiting ATM activity. We performed kinase assays with immunoprecipitated ATM wild type (wt) or ATM kinase dead (kd) from 293T cells, using GST-p53 as a substrate. ATM wt robustly phosphorylated p53 S15, while ATM kd results were

comparable to empty vector (Fig. 15A). Following the addition of purified His-REV7, ATM wt activation of p53 was greatly diminished (Fig. 15B), highlighting REV7's potential involvement in regulating another major pathway of the DDR.

2.2 Materials and Methods

DNA constructs

The human His-REV7 construct (pEtDuet-1-REV7) and pCDH- vectors FH (a FLAG-HA epitope tag on the N- or C-terminus) were obtained from Dr. Richard Wood [43, 44]. The human *ATRIP* wild type (WT) full-length cDNA was obtained from Dr. Minoru Takata [45]. The Flag-*ATR* (pBJF-*ATR*) expression vector were obtained from Dr. Randy Legerski [46]. The human full-length *p53* cDNA was generously provided by Dr. Toshiyuki Habu. GST-CHK1 333-365 cDNA was obtained from GeneScript. The human full-length TopBP1 cDNA was a gift from Dr. Aziz Sancar (Addgene plasmid # 31317) [47]. The Flag-His-*ATM* (wild type: 31985) and Flag-His-*ATM* kd (Kinase dead: 31986) expression vectors were a gift from Dr. Michael Kastan (Addgene plasmid # 31985 and #31986) [48]. pET-MBP/MCS/Thrombin/10xHis vector was obtained from vectorbuilder. After construction, expression vectors were confirmed by DNA sequencing.

ATRIP: GST- full-length ATRIP were PCR amplified from ATRIP-GFP expression vector as a XhoI–NotI fragment with 5′ATRIP (XhoI) primer (5′ - CCGCTCGAGATGGCGGGGACCTCCGCGCCAGGC) and 3′ ATRIP (NotI) primer (5′ - TAAAAGCGGCCGCTCAGCCACACTCCACCTCGGGGTCTTC) to clone into pGEX6P-1 (GE Healthcare). GST-ATRIP 1-107, 1-348, 108-348, 203-348, 203-791, 349-507, 508-791 fragments were PCR amplified from ATRIP-GFP expression vector as a XhoI–NotI fragment

with 5′ATRIP (XhoI) primer (5′ -CCGCTCGAGATGGCGGGGACCTCCGCGCCAGGC) and 3′ ATRIP 107 (NotI) primer (5′ -TAAAAGCGGCCGCTCATGGAACAGTTTCTCTGTTTTTC), 5′ATRIP (XhoI) primer (5′ -CCGCTCGAGATGGCGGGGACCTCCGCGCCAGGC) and 3′ ATRIP 348 (NotI) primer (5′ -TAAAAGCGGCCGCTCATGGTGGCTGCAGGGGGGTGCCAG), 5′ATRIP 108 (XhoI) primer (5′ -CCGCTCGAGATTAAAGATAATTTCGAATTAGAG) and 3′ ATRIP 348 (NotI) primer (5′ -TAAAAGCGGCCGCTCATGGTGGCTGCAGGGGGGTGCCAG), 5′ATRIP 203 (XhoI) primer (5′ -CCGCTCGAGAGGACAAAGCTCCAGACCAGTGAAC) and 3′ ATRIP 348 (NotI) primer (5′ -TAAAAGCGGCCGCTCATGGTGGCTGCAGGGGGGTGCCAG), 5′ATRIP 203 (XhoI) primer (5′ -CCGCTCGAGAGGACAAAGCTCCAGACCAGTGAAC) and 3′ ATRIP (NotI) primer (5′ -TAAAAGCGGCCGCTCAGCCACACTCCACCTCGGGGTCTTC), 5′ATRIP 349 (XhoI) primer (5′ -CCGCTCGAGGGGTTTGGCAGTACCTTGGCTGGAATG) and 3′ ATRIP 507 (NotI) primer (5′ -TAAAAGCGGCCGCTCACCCAGCAGCAGAATCTGCCCC), and 5′ATRIP 508 (XhoI) primer (5′ -CCGCTCGAGGAAGGAAACAGGAGCCTGGTTCAC) and 3′ ATRIP (NotI) primer (5′ -TAAAAGCGGCCGCTCAGCCACACTCCACCTCGGGGTCTTC) to clone into pGEX6P-1 (GE Healthcare). ATRIP RB1 (P235A, P240A)/pGEX6P-1 mutation was introduced using site-directed mutagenesis (TOYOBO KOD FX) and In-Fusion (Takara). The XhoI–NotI fragments from *WT ATRIP* or *ATRIP RB1* (P235A, P240A)/ pGEX6P-1 were inserted into pCDH-EF1□-Flag-HA-MCS-IRES- Puro to generate FH-ATRIP, ATRIP-FH and ATRIP RB1-FH (P235A, P240A).

REV7: REV7 (R124A)/pETDuet-1 mutation was introduced using site-directed mutagenesis (TOYOBO KOD FX) and In-Fusion (Takara).

CHK1: MBP-CHK1 333-365-His were PCR amplified from GST-CHK1 333-365 expression vector as a BamHI–NotI fragment with 5′CHK (BamHI) primer (5′ - CCGAGCTCGGATCCCTCGAGTCATACATTGATAAATTGGTAC) and 3′ CHK1 (NotI) primer (5′ -CGCGGCACCAGGGCGGCCGCCTCACAAGTCTCTTTCAGGCATTG) to clone into pET-MBP/MCS/Thrombin/10xHis.

TopBP1: MBP- full-length TopBP1 -His and MBP-TopBP1 1-1013 -His were PCR amplified from TopBP1 full-length cDNA as a KpnI–NotI fragment with 5′TopBP1 (KpnI) primer (5′ - GGGGTACCATGTCCAGAAATGACAAAGAACCG) and 3′TopBP1 (NotI) primer (5′ - CGCGGCACCAGGGCGGCCGCCTCACAAGTCTCTTTCAGGCATTG) or 3′TopBP1 1013 (NotI) primer (5′ -TAAAAGCGGCCGCTCGACTATTACAGAGCCGGCCATC) to clone into pET-MBP/MCS/Thrombin/10xHis.

p53: full-length p53 was purified as a BamHI–SalI fragment from p53 expression vector and cloned into pGEX6P-1 (GE Healthcare).

ATR: GST-ATR 400-450, 1100-1120, 1120-1230, 1855-1900, 1974-2000 fragments were PCR amplified from ATR expression vector as a XhoI–NotI fragment with 5′ATR 400 (XhoI) primer (5′ - CCGCTCGAGTTGAAAATGGAAAGTATGGAAATC) and 3′ ATR 450 (NotI) primer (5′ - TAAAAGCGGCCGCTCATTCCTCAGTCTGTTTTGGTGCTC), 5′ATR 1100 (XhoI) primer (5′ - CCGCTCGAGTTTGCATCCAGTGATGATCCATATC) and 3′ ATRIP 1120 (NotI) primer (5′ - TAAAAGCGGCCGCTCAAGCCATCAGTTCAGGTGATATG), 5′ATR 1120 (XhoI) primer (5′ - CCGCTCGAGGCTGATTATTTACAACCCAAATTG) and 3′ ATR 1230 (NotI) primer (5′ - TAAAAGCGGCCGCTCAAGTTTCTTTAGGCTGGATGTG), 5′ATR 1855 (XhoI) primer (5′ - CCGCTCGAGCACATGTTATGTGAGTTGGAGCATAG) and 3′ ATR 1900 (NotI) primer (5′ - TAAAAGCGGCCGCTCAGATAGGCTCCTTGGCTCTGTAG), and 5′ATR 1974

(XhoI) primer (5′ - CCGCTCGAGATTGTTCTTCAAAAAGGTGTTG) and 3′ ATRIP 2000 (NotI) primer (5′ - TAAAAGCGGCCGCTCAACCATGGATTAACATGTTCTTAC) to clone into pGEX6P-1 (GE Healthcare).

Mass Spectrometry

Protein identification in the REV7 complex was performed by LC-MS/MS mass spectrometry of gel slices as described [41, 49].

Protein purification

ATR and *ATRIP* fragments were cloned into pGEX-6P-1 vector, transformed into Rosetta E. coli, and grown on LB plates containing carbenicillin (100µg/ml) and chloramphenicol (50µg/ml) overnight at 37 °C. Bulk colonies were added to 600ml Terrific Broth media supplemented with carbenicillin (100µg/ml) and chloramphenicol (50µg/ml), and grown for 3 days at 18°C. Cells were harvested by centrifugation at 5,000 rpm for 20 mins, resuspended in PBS, and centrifuged again at 6,000 rpm for 15 mins. Pellets were stored at -20°C until purification. Pellets were resuspended in 10 volumes of 0.5M buffer C (50mM Tris-HCl (pH8.0), 10% glycerol, 0.5M NaCl, 0.1% Nonidet P-40, 1mM EDTA, 5mM 2-mercaptoethanol) and sonicated on ice (70% amplitude, 50 cycles of 5 seconds with a 10 second pause). The cell lysates were centrifuged at 14,000 rpm for 40 minutes and the supernatants were filtered with a 0.45µm filter. 500µl glutathione sepharose beads were washed and incubated with the filtered supernatant for 1hr rotating at 4°C. The supernatant and resin were loaded to a Poly-Prep chromatography column (Bio-Rad), and beads were washed three times with 5ml of 0.5M buffer C followed by three washes with 4ml of 1M buffer C (50mM Tris-HCl (pH8.0), 10% glycerol,

1M NaCl, 0.1% Nonidet P-40, 1mM EDTA, 5mM 2-mercaptoethanol). The GST-tagged proteins were eluted with 20mM reduced glutathione, frozen in liquid nitrogen, and stored at -80°C.

REV7 and *REV7 (R124A)* mutant were cloned into pETDuet-1, transformed into Rosetta E. coli and grown in 600ml LB medium supplemented with carbenicillin (100μg/ml) and chloramphenicol (50μg/ml) at 37°C with aeration until the culture reached an OD600 value of 0.5. The culture was cooled on ice for 30 mins, and 1mM isopropyl-β-D-thiogalactopyranoside (IPTG) was added. The culture was incubated for an additional 20 hours at 16°C. Cells were then harvested by centrifugation as above, and the pellets were stored at -20°C. Pellets were resuspended in 10 volumes of 1x equilibration buffer (50mM sodium phosphate, 300mM NaCl, 10% glycerol, 0.01% NP-40, pH 7.0) and sonicated on ice (70% amplitude, 50 cycles of 5 sec with a 10 sec pause). The cell lysates were centrifuged at 14,000 rpm for 40 minutes and the supernatants were filtered with a 0.45μm filter. 500μl TALON beads were washed and incubated with the supernatant for 1hr rotating at 4°C. The sample and resin were added to a Poly-Prep chromatography column (Bio-Rad), and washed 3 times with 1ml of 1x equilibration/wash buffer and 5 times with 2ml of 20mM imidazole. The recombinant protein was eluted with 3.2ml of 150mM imidazole, frozen in liquid nitrogen, and stored at -80°C.

Each protein was buffer changed prior to use. Econo-Pac 10DG column (Bio-Rad) was washed with 20ml of buffer containing 100mM Tris (pH 8.0)/100mM NaCl. The protein sample was added to the column, eluted with 4ml of buffer containing 100mM Tris (pH 8.0)/100mM NaCl, frozen in liquid nitrogen and stored at -80°C.

GST Pulldown assay

Purified His-REV7 was added to purified GST-tagged ATR or ATRIP fragments and adjusted to a final volume of 500µl with 0.1B (20mM Tris-HCl(pH8.0), 10% Glycerol, 0.2mM EDTA, 0.1% Tween20, 100mM KCl, 0.007% ME, 0.2mM PMSF, 10mM glycerophosphate). 10µl of washed glutathione sepharose beads were added to the sample and incubated for 2 hours at 4°C. The beads were washed 3 times with 300µl of 0.2B (200 mM KCl, 32 mM Tris-HCl (pH 6.8), 2 mM $MgCl_2$, 16% glycerol, 0.4 mM PMSF, 0.16% Tween-20, 4 mM β-mercaptoethanol, 0.24 mM ED with 20TA), and bound proteins were eluted by boiling in 2× SDS loading buffer (100 mM Tris–HCl [pH 6.8], 4% SDS, 0.2% bromophenol blue, 20% glycerol, 200 mM DTT). Samples were analyzed by SDS-PAGE followed by immunoblotting with anti-MAD2B and anti-GST antibodies.

Immunoprecipitation

293T cells (3.8×10^6) were plated in 10cm dishes 24 hours before transfection with Flag HA tagged *ATRIP* wild type or mutant, or empty vector. 48 hours later, cells were harvested, resuspended in 300µl of 0.5B (500 mM KCl, 20 mM Tris-HCl (pH 8.0), 5 mM $MgCl_2$, 10% glycerol, 1 mM PMSF, 0.1% Tween-20, 10 mM β-mercaptoethanol,) and frozen in liquid nitrogen. Cell pellets were thawed on ice, sonicated (30% amplitude, 4 cycles of 15 seconds with a 30 second pause), and centrifuged (13,000 rpm for 15 minutes). 900 µl of 2B (40 mM Tris-HCl (pH 8.0), 20% glycerol, 0.4 mM ED with 20TA, 0.2% Tween-20) was added to the supernatant and incubated with 10µl of M2-Agarose beads for 2 hours at 4°C. The bound proteins were washed 3 times with 700µl of 0.1B, and eluted with eluted with 30µl of 2x SDS-loading buffer (100 mM Tris-HCl (pH 6.8), 4% SDS, 0.2% bromophenol blue, 20% glycerol and 200 mM

dithiothreitol). Results were analyzed via Western blot using anti-MAD2B and anti-Flag antibodies.

ATR/ATM kinase assays

293T cells (3.8×10^6) were plated in 10cm dishes 24 hours before transfection with Flag tagged *ATR, ATM WT*, or *ATM KD*, or empty vector. 48 hours later, cells were harvested, resuspended in 300µl of 0.5B (500 mM KCl, 20 mM Tris-HCl (pH 8.0), 5 mM MgCl2, 10% glycerol, 1 mM PMSF, 0.1% Tween-20, 10 mM β-mercaptoethanol) and frozen in liquid nitrogen. Cell pellets were thawed on ice, sonicated (30% amplitude, 4 cycles of 15 seconds with a 30 second pause), and centrifuged (13,000 rpm for 15 minutes at 4°C). Supernatants from identical sample types were combined, and 900µl of 2B (40 mM Tris-HCl (pH 8.0), 20% glycerol, 0.4 mM ED with 20TA, 0.2% Tween-20) and 20µl of M2 agarose was added per cell lysate. The solution was incubated for 2 hours rotating at 4°C followed by centrifugation (1500 rpm for 5 minutes at 4°C). The beads were washed twice with 700µl 0.1B (20mM Tris-HCl(pH8.0), 10% Glycerol, 0.2mM EDTA, 0.1% Tween20, 100mM KCl, 0.007% ME, 0.2mM PMSF, 10mM glycerophosphate) per cell lysate and evenly spread into the correct number of tubes per experiment. The beads were washed twice with 700µl of kinase buffer (20 mM HEPES (pH7.6), 10 mM MgCl2, 10 mM MnCl2, 5 mM beta-glycerophosphate, 1 mM NaF). 10µl of His-REV7 or buffer (20 mM HEPES (pH7.6), 0.5 mM DTT) was added, and samples were incubated at 30°C for 15 minutes. 10µl of reaction buffer (20 mM HEPES (pH7.6), 10 mM MgCl2, 10 mM MnCl2, 5 mM beta-glycerophosphate, 1 mM NaF, 1 mM rATP, 5% glycerol, 0.15 µg/µl substrate: purified GST-p53 FL or MBP-Chk1 333-365-His) was added followed by a 30 minute incubation at 30°C. 8µl of 5x SDS loading buffer (250 mM Tris-HCl (pH 6.8), 10% SDS, 1%

bromophenol blue, 50% glycerol and 500 mM dithiothreitol) was added and samples were boiled for 3 minutes at 95°C. Results were analyzed via western blot using the indicated antibodies.

Cell Culture and transfection

Human TK6 (WT, *RAD18*$^{-/-}$ [50], *53BP1*$^{-/-}$ [51], *REV1*$^{-/-}$ (unpublished), and *REV3*$^{-/-}$ [52] cell lines (a gift from Drs Hiroyuki Sasanuma, Tokyo Metropolitan Institute of Medical Scienc and Kouji Hirota, Tokyo Metropolitan Univeristy) were maintained in RPMI- 1640 medium supplemented with 5% horse serum, penicillin/streptomycin, and sodium pyruvate in a 5% CO2 incubator at 37◦C. Human 293T cells were maintained in Dulbecco's modified Eagle's medium (DMEM) supplemented with 10% fetal bovine serum and penicillin/streptomycin in a 5% CO2 incubator at 37°C. Cell transfection was done as described previously [53, 54]. Briefly, 24 or 30μg of plasmid DNA was combined with DMEM (-) and polyethylenimine (PEI), incubated at room temperature for 15 minutes, and then added to cells. 48 hours after transfection, cells were harvested by centrifugation and washed with PBS.

Generation of REV7 deficient TK6 cells

Guide RNA (gRNA) target sequences were described previously [55]. gRNA target sequence (5'- CAGCGTGTGCGATGCCGTCC-3' or 5'- CATCGCACACGCTGATCTTC-3') was inserted in pX330 vector (Addgene, US) for CRISPR Cas9 system. To generate *REV7*$^{-/-}$ for TK6 cells, *REV7-PURO*^{R} and *REV7-HYG*^{R} targeting vectors, a gift from Dr. Hiroyuki Sasanuma [50, 56], were produced from PCR-amplified genomic products combined with *PURO*^{R} and *HYG*^{R} selection marker genes. PCR-amplified genomic products were amplified using the following primers: 5'-

GCGAATTGGGTACCGGGCCAGGGATCCAGGTCTTCTATAATGAG -3' and 5'-CTGGGCTCGAGGGGGGGCCCTCGCAGAGCACATCGGCCACCAC -3' plus 5'-TGGGAAGCTTGTCGACTTAAGGGGGCACCTGCCACCCCACTGATG -3' and 5'-CACTAGTAGGCGCGCCTTAACAGGACCCCAGTTCTAGGCAGGCCC -3' for the left arm and right arm, respectively. Left arm and right arm were inserted into *Apa*I and *Afl*II sites of targeting vectors, respectively, using In-Fusion (Takara). All transfections in TK6 were performed as described [50, 52, 56, 57]. Cells were seeded in 96-well plates and allowed to grow. Resultant colonies were screened for REV7 knockout through western blotting and confirmation of antibiotic resistance integration was analyzed through PCR.

DNA damage experiments

TK6 (WT, *REV7*$^{-/-}$, *RAD18*$^{-/-}$, *53BP1*$^{-/-}$, *REV1*$^{-/-}$, and *REV3*$^{-/-}$) cell lines were spread at a concentration of 2-4 x 105 in T25 flasks and treated with MMC (40 ng/ml), HU (40μM), or control. 24 hours later 4 x 106 cells were harvested, resuspended in 200μl 1x SDS loading buffer (50 mM Tris-HCl (pH 6.8), 2% SDS, 0.1% bromophenol blue, 10% glycerol and 100 mM dithiothreitol) and sonicated (30% amplitude, 4 cycles of 15 seconds with a 30 second pause). Samples were analyzed by western blot using the following antibodies: anti-MAD2B, anti-Tubulin, anti-p-CHK1 S345, and anti-p-p53 S15.

Antibodies

Primary antibodies: p-Chk1 S345, 1:1,000, Cell Signaling (133D3); p-p53 S15, 1:1,000, Cell Signaling (9284); p53, 1:1,000, Cell Signaling (2527S); ATR, 1:400, Cell Signaling (E1S3S); ATRIP, 1:1,000, Cell Signaling (2737S); His-Tag, 1:1,000, Cell Signaling (27E8);

MAD2B, 1:1,200, BD Biosciences (7069948); GST, 1:400, Santa Cruz Biotechnology (K1020); Flag, 1:10,000, Sigma (SLBT6752); αTubulin, 1:8,000, Sigma (047M4760V); Secondary antibodies: Anti-Rabbit, 1:20,000, Li-Cor (C90529-19); Anti-Mouse, 1:20,000, Li-Cor (C90408-08); Anti-Mouse HRP, 1:10,000, Sigma (077M4820V); Anti-Rabbit HRP, 1:10,000, Sigma (028M4755V).

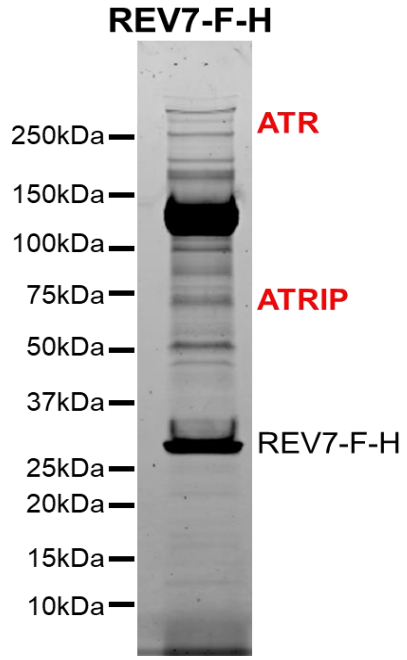

Figure 3. The REV7 complex.
Purification of the REV7 complex with Sypro Ruby staining showing the presence of ATR and ATRIP.

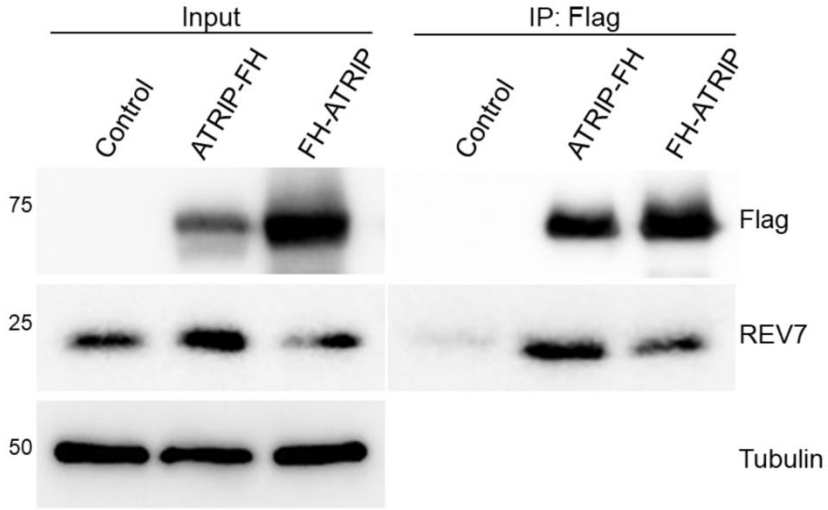

Figure 4. REV7 interacts with ATRIP.
Western blot showing Flag immunoprecipitation of empty vector control, ATRIP-FH, and FH-ATRIP in 293T cells. Endogenous REV7 was detected in ATRIP-FH and FH-ATRIP immunoprecipitates.

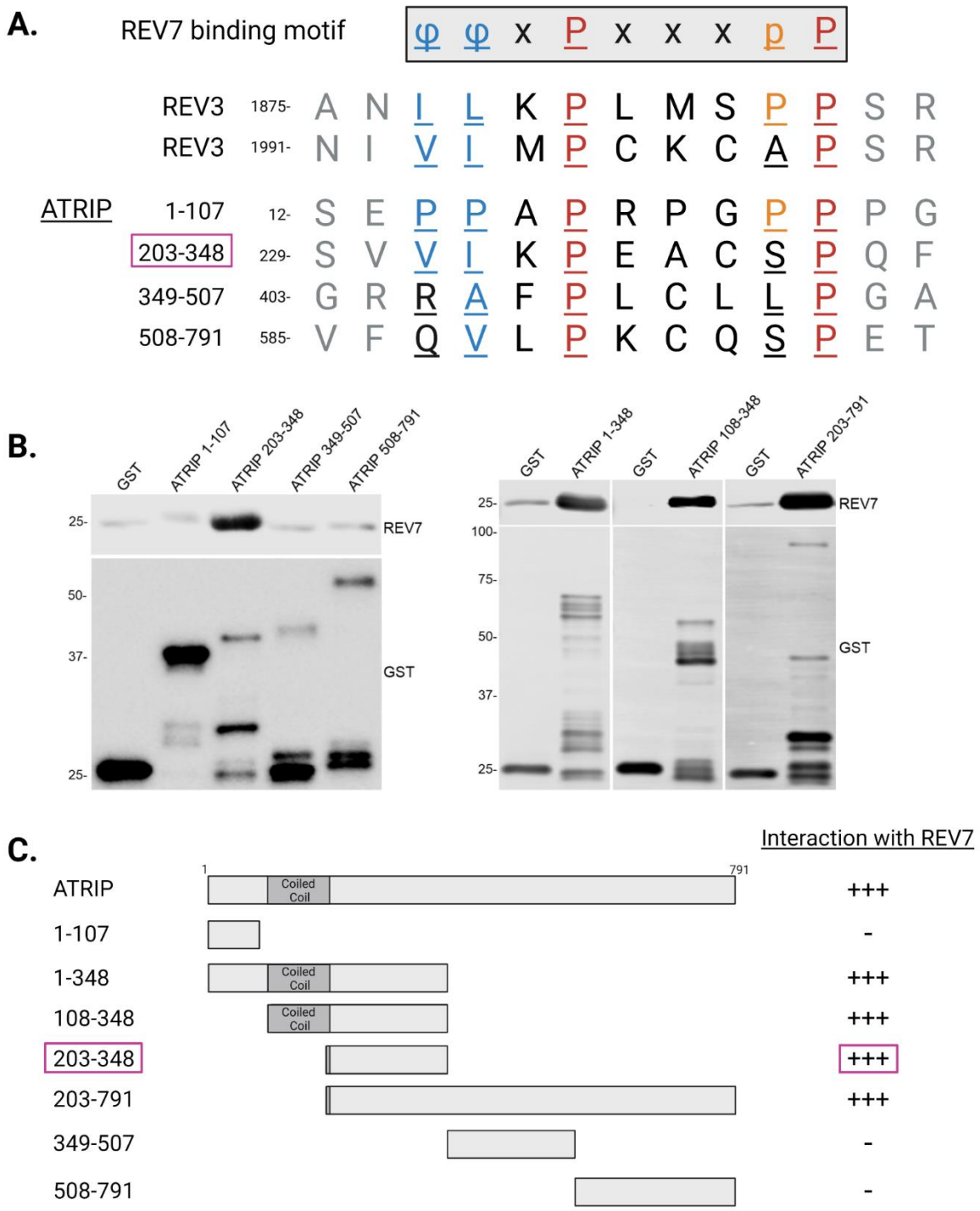

Figure 5. REV7 directly binds to ATRIP 203-348.
A. The conserved REV7 binding motif is shown in the box as φφxPxxxpP. φ is an aliphatic amino acid, x is any amino acid, P is a highly conserved proline, and p is a less conserved proline. We have identified 4 fragments of ATRIP that each contains an RBM.
B. Western blot results of GST-pulldown assays with GST-tagged ATRIP fragments and His-REV7.
C. Schematic of GST-pulldown results with each fragment used in this study.

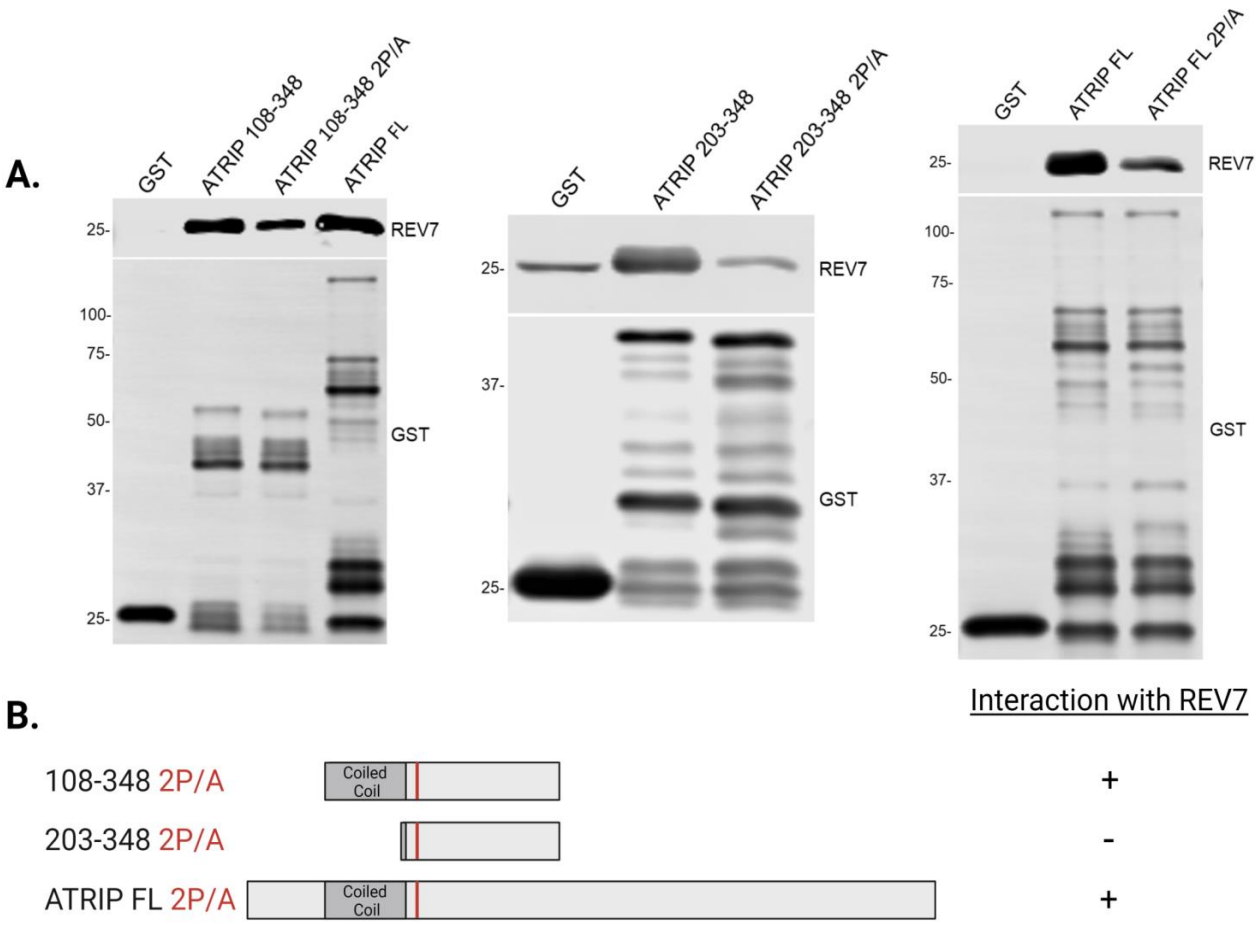

Figure 6. Mutation of ATRIP P235A P240A decreases its interaction with REV7 *in vitro*.
A. Western blot results from GST pulldown assays using ATRIP 108-348, 203-348, and full length harboring a proline to alanine mutation of P235 P240 (2P/A).
B. Schematic representation of ATRIP 2P/A mutants and their interaction with REV7.

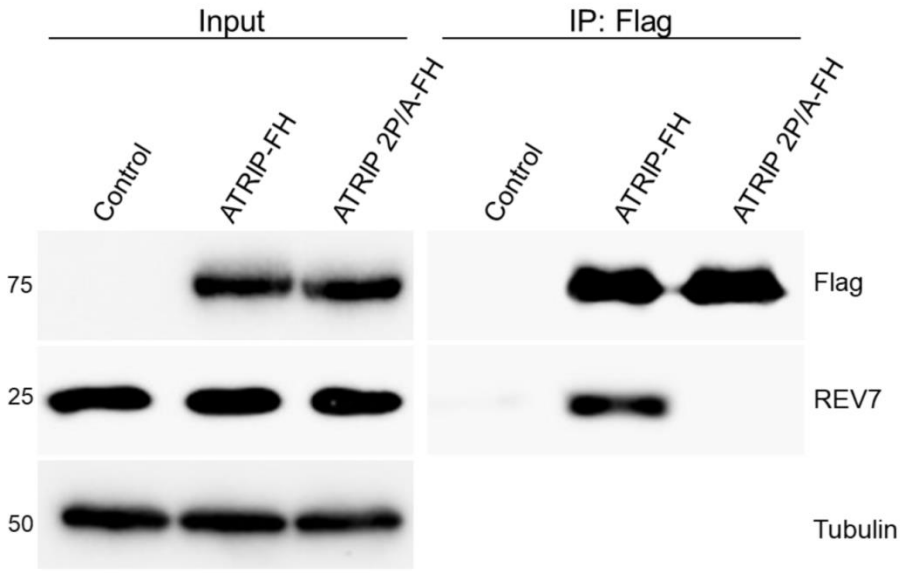

Figure 7. ATRIP P235A P240A does not bind REV7 *in vivo*.
Western blot results of Flag immunoprecipitation of empty vector control, ATRIP-FH, and ATRIP 2P/A-FH in 293T cells.

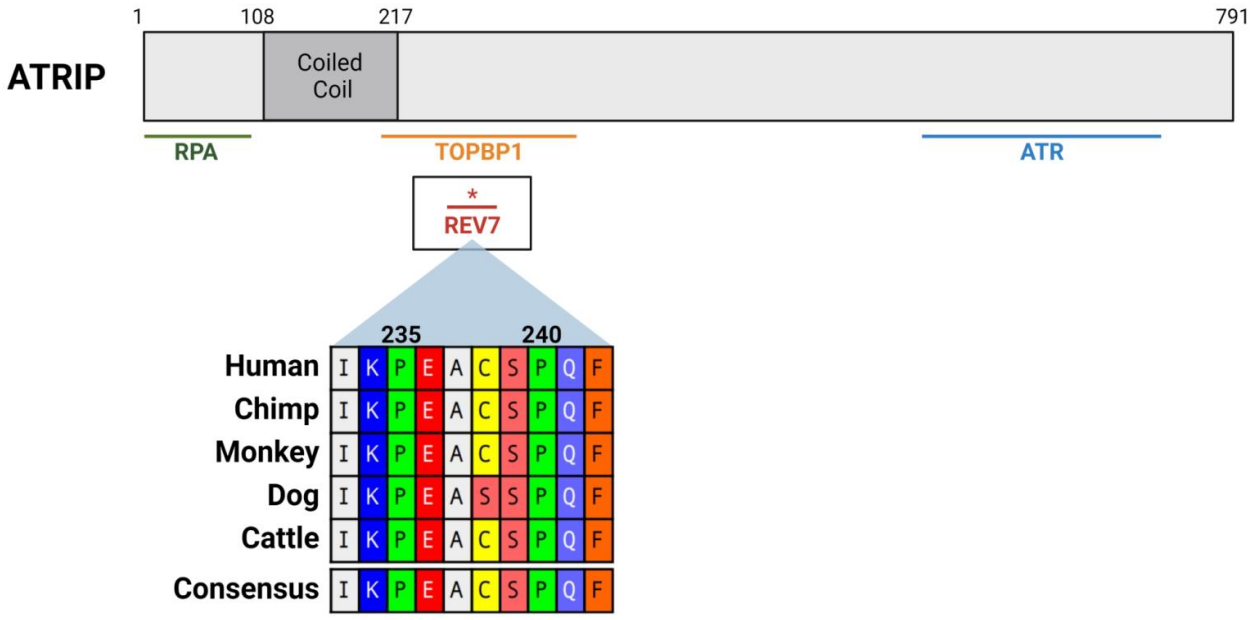

Figure 8. REV7 binding region in ATRIP.
ATRIP protein scheme showing the known binding motifs for RPA, TopBP1, and ATR, with the addition of REV7's binding region in red. Conservation of ATRIP P235 P240 is shown below.

Figure 9. REV7 interacts with ATR.
Western blot results of His pulldown with immunoprecipitated Flag-HA-ATR and purified His-REV7. ATR was detected following His pulldown.

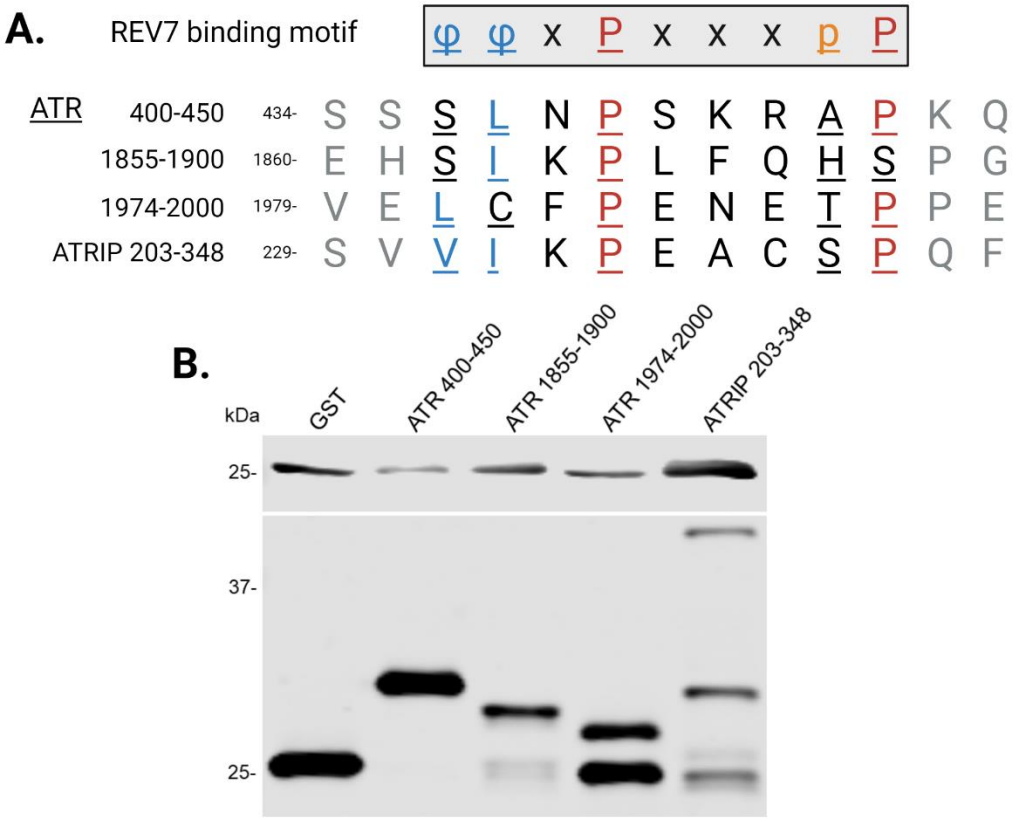

Figure 10. REV7's interaction with ATR fragments.
A. The conserved REV7 binding motif is shown in the box as φφxPxxxpP. We identified 5 fragments of ATR that each contain a possible RBM.
B. Western blot results of GST pulldown assays using GST and GST tagged ATR fragments. ATRIP 203-348 was used as a positive control.

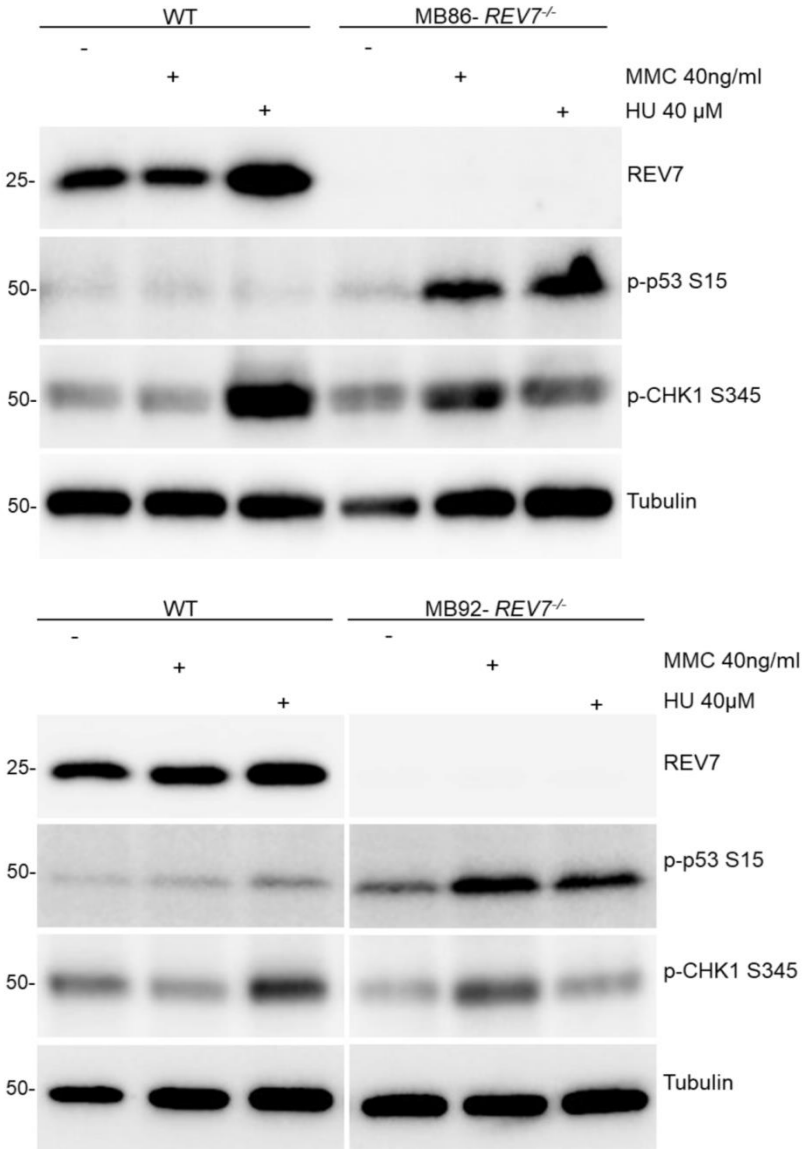

Figure 11. ATR activity in *REV7* KO cells.
WT and *REV7*$^{-/-}$ TK6 cells (MB86 and MB92) were treated with MMC (40ng/ml), HU (40µM), or control. 24 hours after treatment, cells were harvested and lysed by sonication. ATR activity was measured by western blot analysis using p53 S15 and p-CHK1 S345 antibodies.

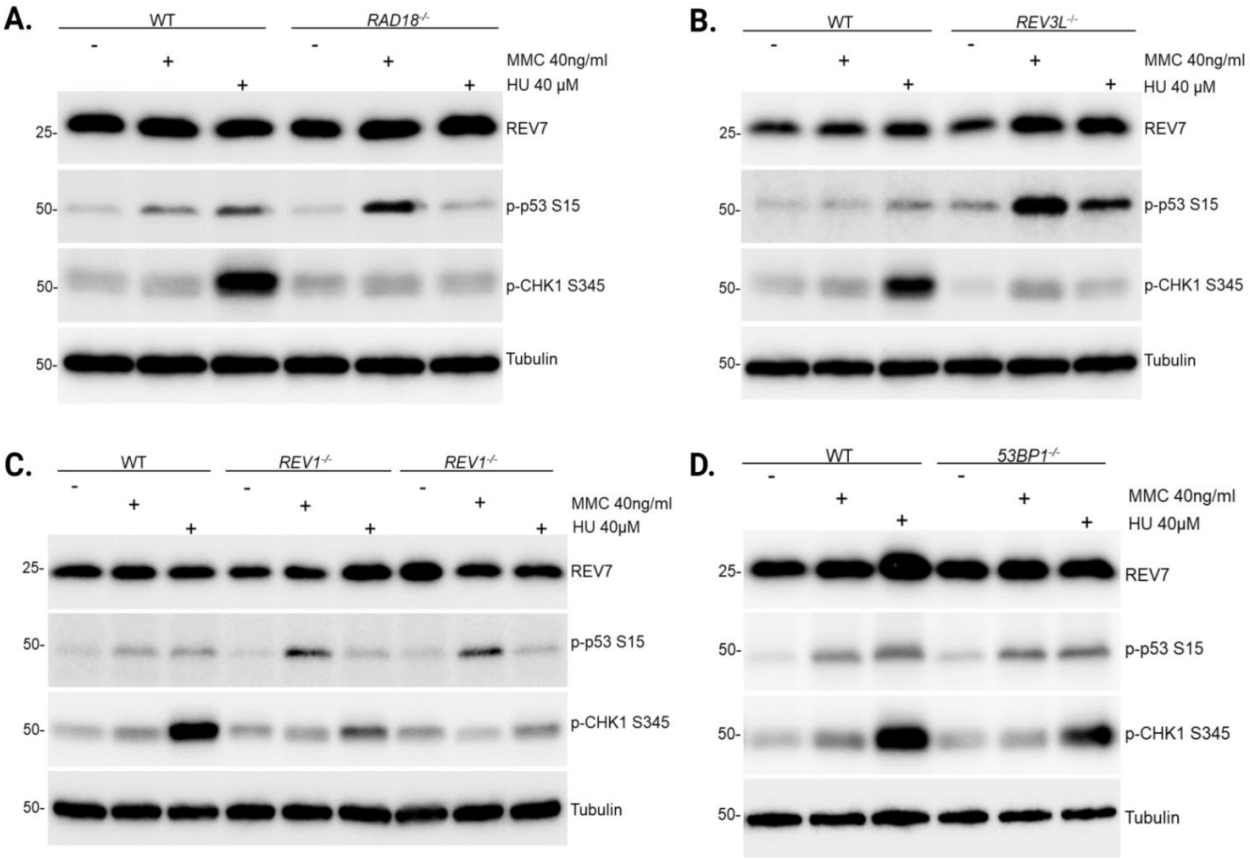

Figure 12. ATR activity in *RAD18, REV3L, REV1,* and *53BP1* KO cells.
A. *RAD18*$^{-/-}$ B. *REV3L*$^{-/-}$ C. *REV1*$^{-/-}$ D. *53BP1*$^{-/-}$ and WT TK6 cells were treated with MMC (40ng/ml), HU (40µM), or control. 24 hours after treatment, cells were harvested and lysed by sonication. ATR activity was measured by western blot analysis using p53 S15 and p-CHK1 S345 antibodies.

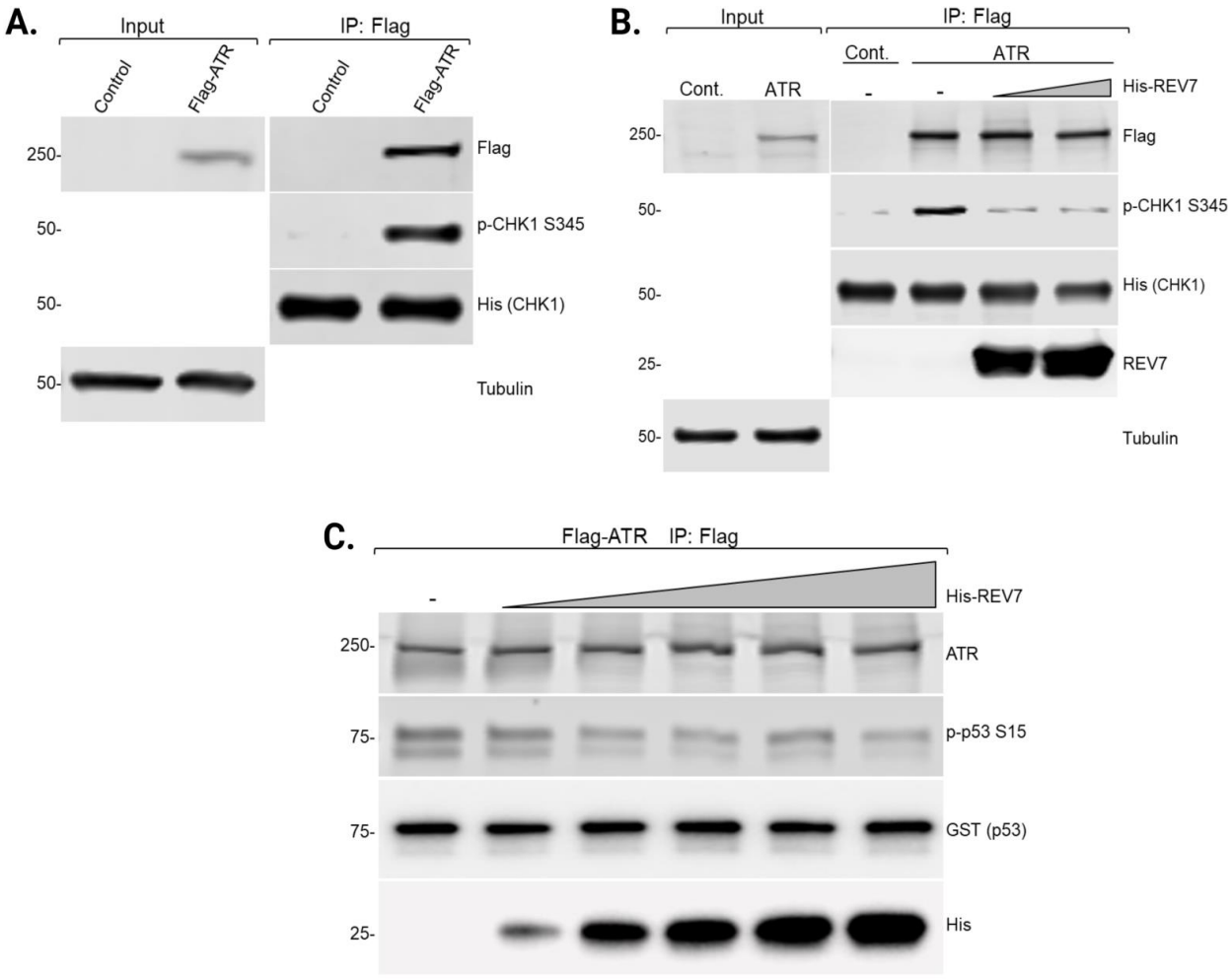

Figure 13. REV7 decreases ATR kinase activity *in vitro*.
293T cells were transfected with Flag tagged ATR or empty vector control. 48 hours after transfection, cells were harvested and immunoprecipitation was carried out using M2 agarose beads.
A. Western blot results of ATR kinase assay with MBP-Chk1 (333-365)-His as a substrate.
B. Western blot results of ATR with MBP-Chk1 (333-365)-His as a substrate, with the addition of 0, 5, or 10µl of His-REV7.
C. Western blot results of ATR kinase assay with GST-p53 as a substrate, with the addition of 0, 2, 4, 6, 8, or 10µl of His-REV7.

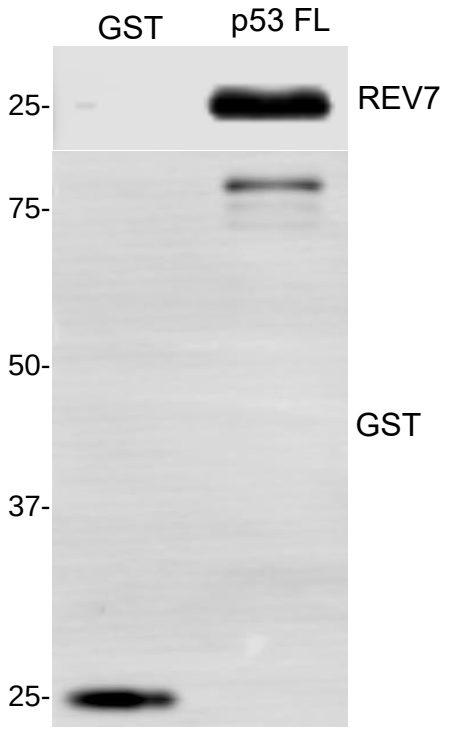

Figure 14. REV7 directly interacts with p53.
Western blot results from GST pulldown assay with GST-p53 and His-REV7. Purified GST was used as a negative control. Following electrophoresis, samples were immunoblotted with anti-REV7 and anti-GST antibodies as indicated.

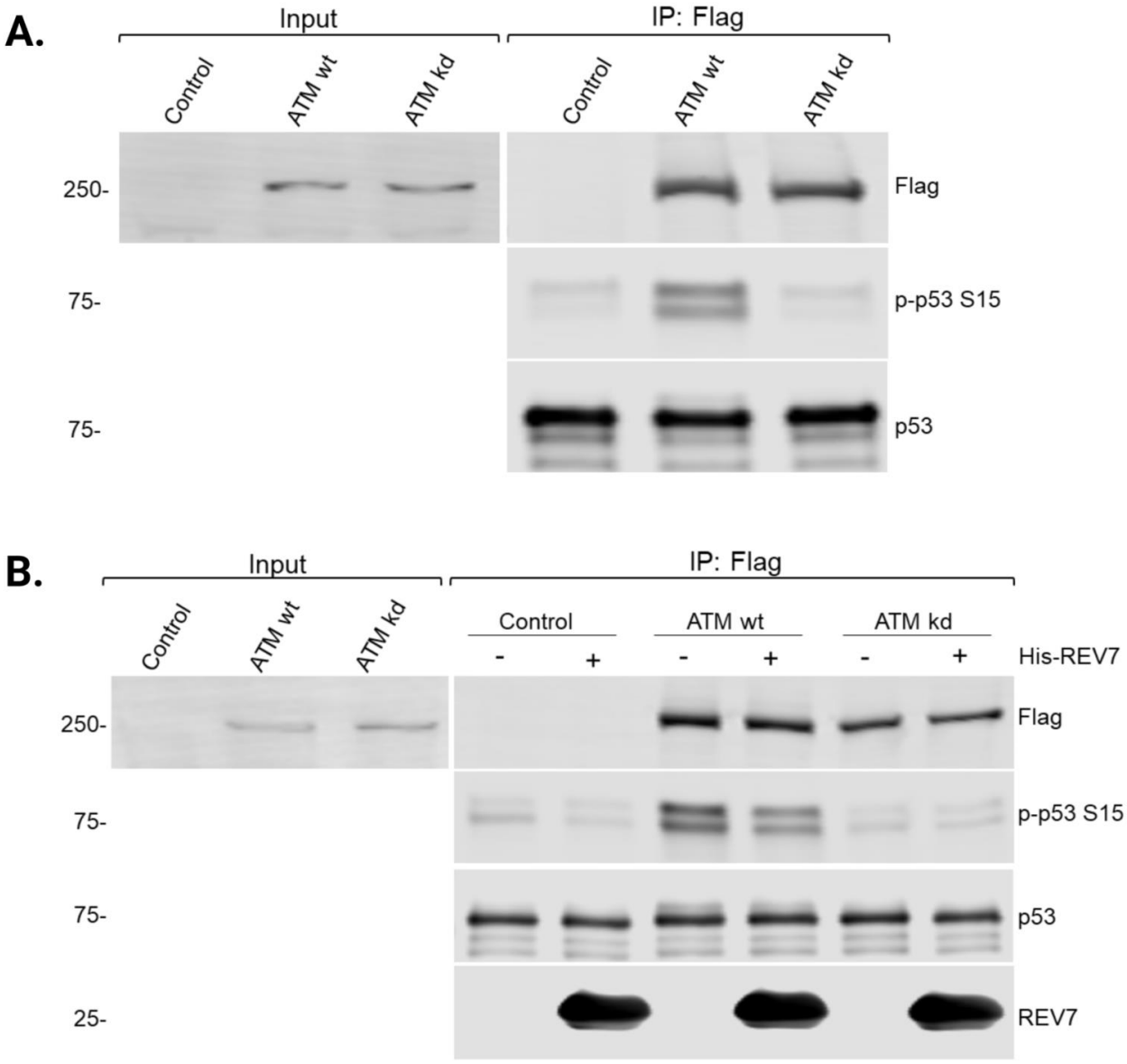

Figure 15. REV7 decreases ATM kinase activity *in vitro*.
293T cells were transfected with Flag tagged ATM wild type (wt), ATM kinase dead (kd), or empty vector control. 48 hours after transfection, cells were harvested and immunoprecipitation was carried out using M2 agarose beads.
A. Western blot results of ATM kinase assay with GST-p53 as a substrate.
B. Western blot results of ATM kinase assay using GST-p53 as a substrate with the addition of 0 or 10µl of His-REV7.

CHAPTER 3: DISCUSSION AND FUTURE DIRECTIONS

This study revealed a novel interaction between ATRIP and REV7 and pinpointed the interaction to two amino acids on ATRIP (P235, P240). Mutation of these two prolines to alanine (2P/A) abolishes the interaction between REV7 and ATRIP in the cell, however, slight binding is retained *in vitro* at ATRIP's coiled coil region 108-217 (Figs. 5-7). This difference may arise due to disruption of the normal dynamics of ATRIP dimerization by the incorporation of the N terminal GST tag in our recombinant ATRIP protein. However, *in vivo,* ATRIP dimerization may block REV7's access to ATRIP's coiled coil region, which could explain why endogenous REV7 did not immunoprecipitate with ATRIP FL 2P/A. Another possibility is provided by post translational modification by ATR [58] or CDK2 [59]. The phosphorylated ATRIP may inhibit interaction with REV7 at the coiled coil region. The coiled coil region does not contain an RBM, so it does not likely interact with REV7's seatbelt domain, but it may interact with another REV7 domain [31, 60]. Aside from its seatbelt interactions at ATRIP (P235, P240), REV7 contains additional surfaces that facilitate protein binding including a dimerization domain and REV1 binding domain. To determine whether the REV7 dimerization domain is necessary for ATRIP binding, we confirmed the ability of REV7 dimerization mutant R124A to bind ATRIP (Fig. 16). Additionally, we would like to test if REV7 containing a mutated REV1 binding site is still capable of binding ATRIP 2P/A. These studies should reveal whether ATRIP contains an additional REV7 binding site in its coiled coil region.

Analysis of ATR activity in a variety of knockout cells following DNA damage shows that REV7 likely has a function outside of the 53BP1 pathway and TLS pathway. Our data show that *REV7* KOs uniquely display increased phosphorylation of CHK1 S345 following MMC treatment, placing a role of REV7 in the ATR pathway (Fig. 11). RAD18, REV1, and REV3L

each have vital functions in the TLS pathway. All three of these KO cell lines showed increased p53 S15 following treatment with MMC (Fig. 12), suggesting increased phosphorylation of p53 could be a result of a defective TLS pathway. Since *REV7* KO cells also showed increased p53 S15 following MMC treatment, this phenotype may be dependent on REV7's role in TLS. However, we have shown that REV7 directly binds p53 and inhibits phosphorylation of S15 *in vitro* (Figs. 13-15). Therefore, the REV7-p53 interaction may become unstable without TLS pathway activation or TLS proteins.

HU treatment did not induce p53 phosphorylation in *RAD18* or *REV1* KO cells, however, it did increase p53 S15 levels in *REV3L* and *REV7* KO cells even though pol ζ is downstream of RAD18 and REV1 in the TLS pathway. Therefore, an explanation for increased p53 activity in our *REV7* KO cells could be the lack of REV7 inhibition of p53. Since *REV3L* KOs also show this phenotype, it's possible that REV3L plays a role in stabilizing the interaction between p53 and REV7. In this case, loss of REV7 or REV3L would result in hyperactive p53. We did not observe any increase in CHK1 S345 in *RAD18*, *REV1*, *REV7*, or *REV3L* knockout cells, suggesting p53 plays a more prominent role than CHK1 if the TLS pathway is inactive.

53BP1 KOs did not show significant variations in ATR signaling compared to WT cells (Fig. 12D). 53BP1 is an important factor in DSB repair by NHEJ, as it directly recruits components of the Shieldin complex including REV7 [33]. Thus, increased ATR activity in *REV7* KO cells was not likely due to REV7's role in the Shieldin complex.

While these studies have been fruitful, KO of *REV7* impairs multiple pathways which may mask our ability to make further conclusions surrounding REV7's direct involvement in the ATR pathway. Therefore, we would like examine the effects of ATRIP 2P/A on ATR activity in a biological setting, as we have shown that ATRIP 2P/A does not directly interact with REV7 *in*

vivo. ATRIP P235 and P240 are evolutionarily conserved from cattle to humans (Fig. 8); however, they are not conserved in other mammals including mice and chickens. This is an intriguing observation, as it implies a more recently acquired function of ATRIP that has yet to be explored. A previous project in our lab generated ATRIP conditional knockouts in the DT40 cell line [61]. We have stably expressed human ATRIP or ATRIP 2P/A in these cells (Fig. 17) and plan to analyze ATR activity following DNA damage treatment. Since ATRIP P235 P240 is not originally conserved in DT40 cells, it will be interesting to see how ATR activity is influenced. We expect that expression of wild type human ATRIP will suppress ATR activity, while no difference will be seen with ATRIP 2P/A expression. We also plan to assess effects of ATRIP 2P/A through two alternative methods. We have obtained ATRIP shRNA and are currently testing knockdown efficiency in 293T cells co-transfected with FH-ATRIP (Fig. 18). We plan to knockdown endogenous ATRIP followed by expression of shRNA resistant WT and 2P/A ATRIP cDNA. Additionally, we will use CRISPR-Cas9 to knock in ATRIP 2P/A in the TK6 cell line. Analysis of ATR activity in these cell lines compared to REV7 KOs will provide further insight on the distinct role of REV7 in the ATR pathway. Furthermore, we would like to explore ATR activity over different time points following DNA damage. In this study, cells were harvested 24 hours following MMC or HU treatment, but analysis of shorter and longer treatment times may help elucidate which steps in the ATR pathway include REV7 regulation. If REV7 only affects initial ATR signaling, we may only be able to detect phenotypic differences prior to 24 hours. We suspect that initial ATR signaling will be increased in ATRIP 2P/A cell lines compared to wild type. It will also be interesting to explore effects of ATRIP 2P/A in different cell lines. For example, U2OS cells are deficient in the ATR activator ETAA1. If REV7

competes with TopBP1 binding to ATRIP, we may see a more significant phenotype in U2OS cells since ATR activation relies more heavily on TopBP1.

Through *in vitro* kinase assays, we have shown REV7 directly attenuates ATR phosphorylation of p53 S15 and CHK1 S345 (Fig. 13). We will need to conduct future kinase assays since we have only analyzed REV7's effect on basal levels of ATR activity. We plan to perform kinase assays with the addition of TopBP1 and other factors (ssDNA, RPA, 9-1-1 complex, etc.) to elucidate the mechanism of REV7 binding and inhibition on full activation of the ATR pathway. REV7's ability to inhibit ATR in the presence of other factors will help determine where in the ATR pathway REV7 regulation takes place.

REV7 binds to ATRIP in its TopBP1 binding region (203-348), however, it is unknown whether REV7 and TopBP1 are able to bind ATRIP simultaneously or whether one has a higher binding affinity. To address this issue, we plan to conduct pulldown assays with the addition of TopBP1. We have already purified MBP-TopBP1-His (Supplementary Fig. 1) which will be used in combination with His-REV7 and GST-ATRIP to determine binding mechanisms. Since TopBP1 was not found in mass spectrometry analysis of the REV7 complex, we do not suspect REV7 and TopBP1 are able to concurrently bind ATRIP. Additional immunoprecipitation experiments of ATRIP following DNA damage could provide further insight into the mechanisms of TopBP1 and REV7 binding. We anticipate REV7's association with ATRIP will diminish following DNA damage to permit binding and activation of the ATR complex by TopBP1.

The novel interaction between REV7 and p53 is of great significance, as p53 is a major tumor suppressor and heavily involved in maintaining genome integrity. Over 50% of cancers harbor a mutation in *p53* [62]. Therefore, future studies looking into REV7's regulation of p53

are clinically pertinent. We have identified multiple RBMs in p53 and plan to generate p53 mutants deficient in REV7 binding. These mutants will be used to investigate the effects of REV7 on p53 functions including regulation of cell cycle checkpoints, apoptosis, and transcriptional activity.

Finally, we propose an overall model of the ATR pathway in which REV7 is initially bound to the ATR complex through ATRIP in order to prevent unwarranted ATR signaling. Following DNA damage or replication stress, REV7 uncouples from ATRIP and allows complete activation of the ATR complex (Fig. 19). Determining whether TopBP1 or other factors specifically displace REV7 will need further investigation. Additionally, we propose a second mechanism of DDR regulation by which REV7 directly binds to key substrates including p53, limiting access of ATM and ATR (Fig. 19). Taken together, this work has identified REV7 as a potential master regulator of the DDR and highlights a novel role of REV7 in preserving genome integrity.

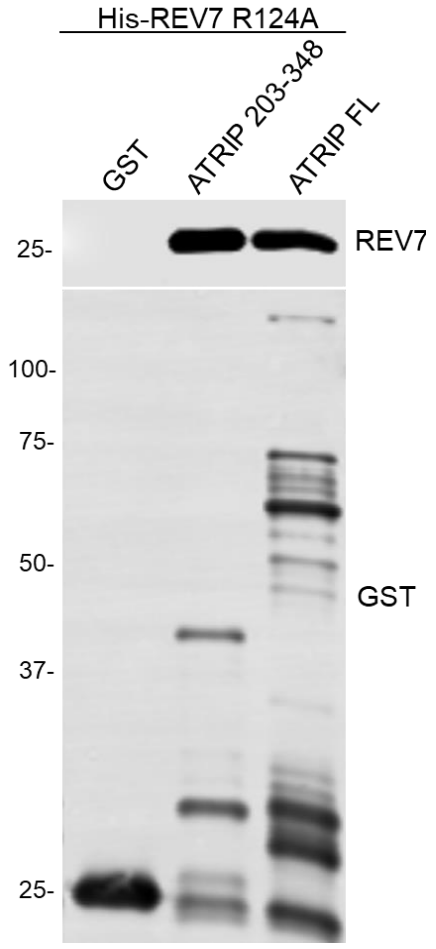

Figure 16. REV7 dimerization mutant interacts with ATRIP.
Western blot results from GST pulldown assay with GST-ATRIP 203-348 and GST-ATRIP FL with His-REV7 dimerization mutant R124A. Purified GST was used as a negative control.

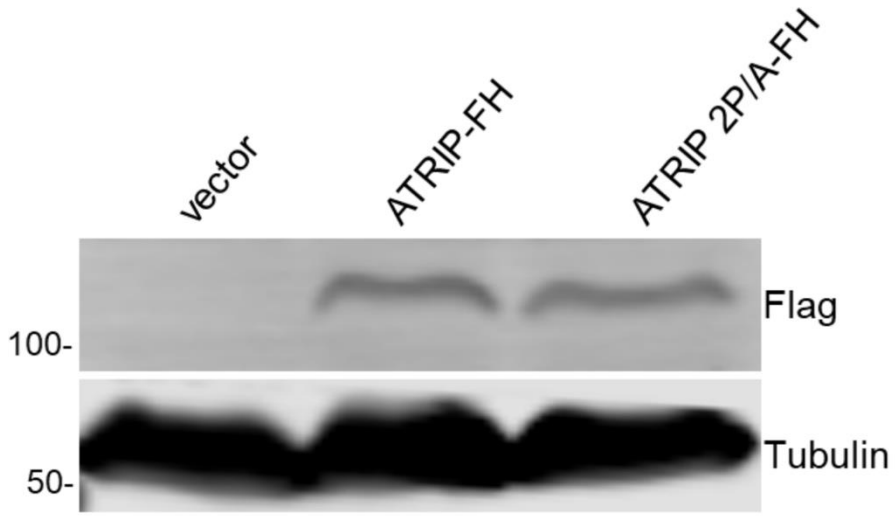

Figure 17. DT40 ATRIP conditional KO cells expressing empty vector, ATRIP-FH, or ATRIP 2P/A-FH.
48 hours following transfection, DT40 cells were harvested, sonicated, and immunoblotted with the indicated antibodies.

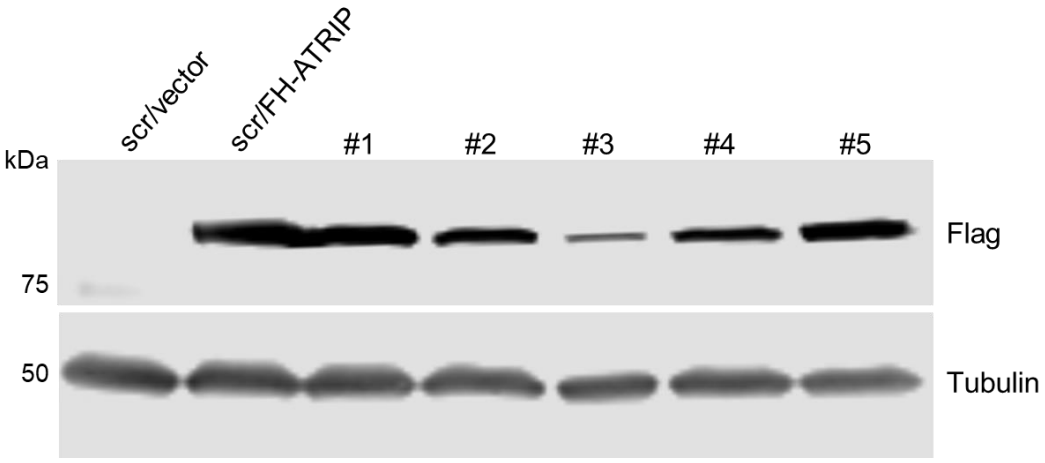

Figure 18. **ATRIP shRNA knockdown efficiency**.
293T cells were co-transfected with control ATRIP shRNA (Scr) or ATRIP shRNA, and either empty vector control or FH-ATRIP. Knockdown ability of ATRIP shRNA #1-5 were measured via western blot using anti-Flag antibodies.
Results obtained with Justin Clark.

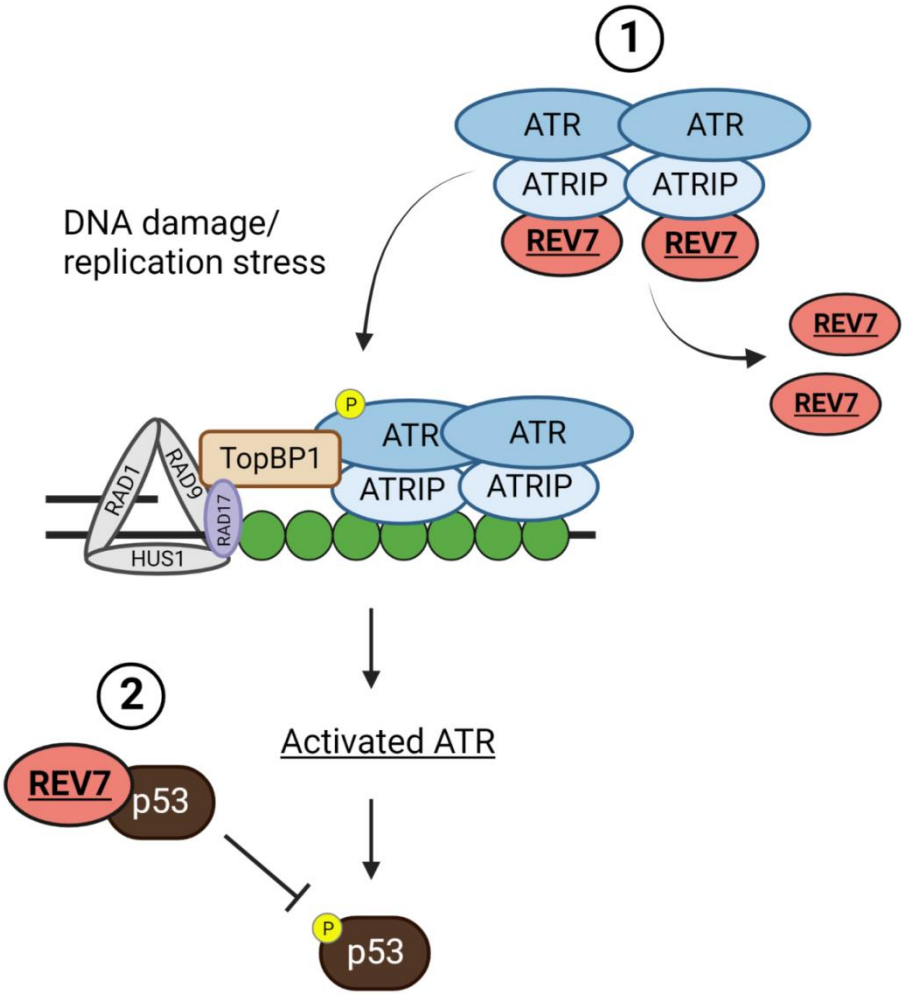

Figure 19. **Proposed mechanism of REV7 regulation of the ATR pathway**. 1) REV7 is bound to the ATR-ATRIP complex to limit ATR signaling prior to DNA damage or replication stress. Upon recruitment of ATR-ATRIP to sites of damage, REV7 uncouples from ATRIP. 2) REV7 directly binds substrates including p53 and inhibits activation by DDR transducers (ATR/ATM).

REFERENCES

1. Ciccia, A. and S.J. Elledge, *The DNA damage response: making it safe to play with knives.* Mol Cell, 2010. **40**(2): p. 179-204.
2. O'Neill, T., et al., *Utilization of oriented peptide libraries to identify substrate motifs selected by ATM.* J Biol Chem, 2000. **275**(30): p. 22719-27.
3. Lempiainen, H. and T.D. Halazonetis, *Emerging common themes in regulation of PIKKs and PI3Ks.* EMBO J, 2009. **28**(20): p. 3067-73.
4. Lovejoy, C.A. and D. Cortez, *Common mechanisms of PIKK regulation.* DNA Repair (Amst), 2009. **8**(9): p. 1004-8.
5. Cimprich, K.A. and D. Cortez, *ATR: an essential regulator of genome integrity.* Nat Rev Mol Cell Biol, 2008. **9**(8): p. 616-27.
6. Brown, E.J. and D. Baltimore, *ATR disruption leads to chromosomal fragmentation and early embryonic lethality.* Genes Dev, 2000. **14**(4): p. 397-402.
7. Halazonetis, T.D., V.G. Gorgoulis, and J. Bartek, *An oncogene-induced DNA damage model for cancer development.* Science, 2008. **319**(5868): p. 1352-5.
8. Gorecki, L., et al., *Discovery of ATR kinase inhibitor berzosertib (VX-970, M6620): Clinical candidate for cancer therapy.* Pharmacol Ther, 2020. **210**: p. 107518.
9. Hall, A.B., et al., *Potentiation of tumor responses to DNA damaging therapy by the selective ATR inhibitor VX-970.* Oncotarget, 2014. **5**(14): p. 5674-85.
10. Reaper, P.M., et al., *Selective killing of ATM- or p53-deficient cancer cells through inhibition of ATR.* Nat Chem Biol, 2011. **7**(7): p. 428-30.
11. Zou, L. and S.J. Elledge, *Sensing DNA damage through ATRIP recognition of RPA-ssDNA complexes.* Science, 2003. **300**(5625): p. 1542-8.
12. Fanning, E., V. Klimovich, and A.R. Nager, *A dynamic model for replication protein A (RPA) function in DNA processing pathways.* Nucleic Acids Res, 2006. **34**(15): p. 4126-37.
13. Yan, S. and W.M. Michael, *TopBP1 and DNA polymerase-alpha directly recruit the 9-1-1 complex to stalled DNA replication forks.* J Cell Biol, 2009. **184**(6): p. 793-804.
14. Delacroix, S., et al., *The Rad9-Hus1-Rad1 (9-1-1) clamp activates checkpoint signaling via TopBP1.* Genes Dev, 2007. **21**(12): p. 1472-7.
15. Ohashi, E., et al., *Interaction between Rad9-Hus1-Rad1 and TopBP1 activates ATR-ATRIP and promotes TopBP1 recruitment to sites of UV-damage.* DNA Repair (Amst), 2014. **21**: p. 1-11.
16. Feng, S., et al., *Ewing Tumor-associated Antigen 1 Interacts with Replication Protein A to Promote Restart of Stalled Replication Forks.* J Biol Chem, 2016. **291**(42): p. 21956-21962.
17. Haahr, P., et al., *Activation of the ATR kinase by the RPA-binding protein ETAA1.* Nat Cell Biol, 2016. **18**(11): p. 1196-1207.
18. Kobayashi, M., et al., *NBS1 directly activates ATR independently of MRE11 and TOPBP1.* Genes Cells, 2013. **18**(3): p. 238-46.
19. Matsuoka, S., et al., *ATM and ATR substrate analysis reveals extensive protein networks responsive to DNA damage.* Science, 2007. **316**(5828): p. 1160-6.

20. Lukas, J., C. Lukas, and J. Bartek, *Mammalian cell cycle checkpoints: signalling pathways and their organization in space and time.* DNA Repair (Amst), 2004. **3**(8-9): p. 997-1007.
21. Lane, D.P., *Cancer. p53, guardian of the genome.* Nature, 1992. **358**(6381): p. 15-6.
22. Helton, E.S. and X. Chen, *p53 modulation of the DNA damage response.* J Cell Biochem, 2007. **100**(4): p. 883-96.
23. Zhao, H. and H. Piwnica-Worms, *ATR-mediated checkpoint pathways regulate phosphorylation and activation of human Chk1.* Mol Cell Biol, 2001. **21**(13): p. 4129-39.
24. Tibbetts, R.S., et al., *A role for ATR in the DNA damage-induced phosphorylation of p53.* Genes Dev, 1999. **13**(2): p. 152-7.
25. Pfleger, C.M., et al., *Inhibition of Cdh1-APC by the MAD2-related protein MAD2L2: a novel mechanism for regulating Cdh1.* Genes Dev, 2001. **15**(14): p. 1759-64.
26. Lawrence, C.W., *Cellular roles of DNA polymerase zeta and Rev1 protein.* DNA Repair (Amst), 2002. **1**(6): p. 425-35.
27. Boersma, V., et al., *MAD2L2 controls DNA repair at telomeres and DNA breaks by inhibiting 5' end resection.* Nature, 2015. **521**(7553): p. 537-40.
28. Xu, G., et al., *REV7 counteracts DNA double-strand break resection and affects PARP inhibition.* Nature, 2015. **521**(7553): p. 541-4.
29. Rosenberg, S.C. and K.D. Corbett, *The multifaceted roles of the HORMA domain in cellular signaling.* J Cell Biol, 2015. **211**(4): p. 745-55.
30. Hanafusa, T., et al., *Overlapping in short motif sequences for binding to human REV7 and MAD2 proteins.* Genes Cells, 2010. **15**(3): p. 281-96.
31. Rizzo, A.A., et al., *Rev7 dimerization is important for assembly and function of the Rev1/Polzeta translesion synthesis complex.* Proc Natl Acad Sci U S A, 2018. **115**(35): p. E8191-E8200.
32. Murakumo, Y., et al., *A human REV7 homolog that interacts with the polymerase zeta catalytic subunit hREV3 and the spindle assembly checkpoint protein hMAD2.* J Biol Chem, 2000. **275**(6): p. 4391-7.
33. Gupta, R., et al., *DNA Repair Network Analysis Reveals Shieldin as a Key Regulator of NHEJ and PARP Inhibitor Sensitivity.* Cell, 2018. **173**(4): p. 972-988 e23.
34. de Krijger, I., et al., *MAD2L2 dimerization and TRIP13 control shieldin activity in DNA repair.* Nat Commun, 2021. **12**(1): p. 5421.
35. Lawrence, C.W., G. Das, and R.B. Christensen, *REV7, a new gene concerned with UV mutagenesis in yeast.* Mol Gen Genet, 1985. **200**(1): p. 80-5.
36. Makarova, A.V., J.L. Stodola, and P.M. Burgers, *A four-subunit DNA polymerase zeta complex containing Pol delta accessory subunits is essential for PCNA-mediated mutagenesis.* Nucleic Acids Res, 2012. **40**(22): p. 11618-26.
37. Baranovskiy, A.G., et al., *DNA polymerase delta and zeta switch by sharing accessory subunits of DNA polymerase delta.* J Biol Chem, 2012. **287**(21): p. 17281-17287.
38. Kikuchi, S., et al., *Structural basis of recruitment of DNA polymerase zeta by interaction between REV1 and REV7 proteins.* J Biol Chem, 2012. **287**(40): p. 33847-52.
39. Martin, S.K. and R.D. Wood, *DNA polymerase zeta in DNA replication and repair.* Nucleic Acids Res, 2019. **47**(16): p. 8348-8361.
40. Gao, S., et al., *An OB-fold complex controls the repair pathways for DNA double-strand breaks.* Nat Commun, 2018. **9**(1): p. 3925.

41. Tomida, J., et al., *FAM35A associates with REV7 and modulates DNA damage responses of normal and BRCA1-defective cells.* EMBO J, 2018. **37**(12).
42. Ghezraoui, H., et al., *53BP1 cooperation with the REV7-shieldin complex underpins DNA structure-specific NHEJ.* Nature, 2018. **560**(7716): p. 122-127.
43. Tomida, J., et al., *REV7 is essential for DNA damage tolerance via two REV3L binding sites in mammalian DNA polymerase zeta.* Nucleic Acids Res, 2015. **43**(2): p. 1000-11.
44. Yousefzadeh, M.J., et al., *Mechanism of suppression of chromosomal instability by DNA polymerase POLQ.* PLoS Genet, 2014. **10**(10): p. e1004654.
45. Tomida, J., et al., *A novel interplay between the Fanconi anemia core complex and ATR-ATRIP kinase during DNA cross-link repair.* Nucleic Acids Res, 2013. **41**(14): p. 6930-41.
46. Zhang, N., et al., *Cdc5L interacts with ATR and is required for the S-phase cell-cycle checkpoint.* EMBO Rep, 2009. **10**(9): p. 1029-35.
47. Lindsey-Boltz, L.A. and A. Sancar, *Tethering DNA damage checkpoint mediator proteins topoisomerase IIbeta-binding protein 1 (TopBP1) and Claspin to DNA activates ataxia-telangiectasia mutated and RAD3-related (ATR) phosphorylation of checkpoint kinase 1 (Chk1).* J Biol Chem, 2011. **286**(22): p. 19229-36.
48. Canman, C.E., et al., *Activation of the ATM kinase by ionizing radiation and phosphorylation of p53.* Science, 1998. **281**(5383): p. 1677-9.
49. Takata, K., et al., *Human DNA helicase HELQ participates in DNA interstrand crosslink tolerance with ATR and RAD51 paralogs.* Nat Commun, 2013. **4**: p. 2338.
50. Tsuda, M., et al., *The dominant role of proofreading exonuclease activity of replicative polymerase epsilon in cellular tolerance to cytarabine (Ara-C).* Oncotarget, 2017. **8**(20): p. 33457-33474.
51. Sasanuma, H., et al., *BRCA1 ensures genome integrity by eliminating estrogen-induced pathological topoisomerase II-DNA complexes.* Proc Natl Acad Sci U S A, 2018. **115**(45): p. E10642-E10651.
52. Saha, L.K., et al., *Differential micronucleus frequency in isogenic human cells deficient in DNA repair pathways is a valuable indicator for evaluating genotoxic agents and their genotoxic mechanisms.* Environ Mol Mutagen, 2018. **59**(6): p. 529-538.
53. Aricescu, A.R., W. Lu, and E.Y. Jones, *A time- and cost-efficient system for high-level protein production in mammalian cells.* Acta Crystallogr D Biol Crystallogr, 2006. **62**(Pt 10): p. 1243-50.
54. Lee, Y.S., M.T. Gregory, and W. Yang, *Human Pol zeta purified with accessory subunits is active in translesion DNA synthesis and complements Pol eta in cisplatin bypass.* Proc Natl Acad Sci U S A, 2014. **111**(8): p. 2954-9.
55. Shalem, O., et al., *Genome-scale CRISPR-Cas9 knockout screening in human cells.* Science, 2014. **343**(6166): p. 84-87.
56. Kratz, K., et al., *FANCD2-Associated Nuclease 1 Partially Compensates for the Lack of Exonuclease 1 in Mismatch Repair.* Mol Cell Biol, 2021. **41**(9): p. e0030321.
57. Ibrahim, M.A., et al., *Enhancing the sensitivity of the thymidine kinase assay by using DNA repair-deficient human TK6 cells.* Environ Mol Mutagen, 2020. **61**(6): p. 602-610.
58. Cortez, D., et al., *ATR and ATRIP: partners in checkpoint signaling.* Science, 2001. **294**(5547): p. 1713-6.

59. Myers, J.S., et al., *Cyclin-dependent kinase 2 dependent phosphorylation of ATRIP regulates the G2-M checkpoint response to DNA damage.* Cancer Res, 2007. **67**(14): p. 6685-90.
60. Hara, K., et al., *Crystal structure of human REV7 in complex with a human REV3 fragment and structural implication of the interaction between DNA polymerase zeta and REV1.* J Biol Chem, 2010. **285**(16): p. 12299-307.
61. Shigechi, T., et al., *ATR-ATRIP kinase complex triggers activation of the Fanconi anemia DNA repair pathway.* Cancer Res, 2012. **72**(5): p. 1149-56.
62. Ozaki, T. and A. Nakagawara, *Role of p53 in Cell Death and Human Cancers.* Cancers (Basel), 2011. **3**(1): p. 994-1013.

APPENDIX A: SUPPLEMENTARY FIGURES

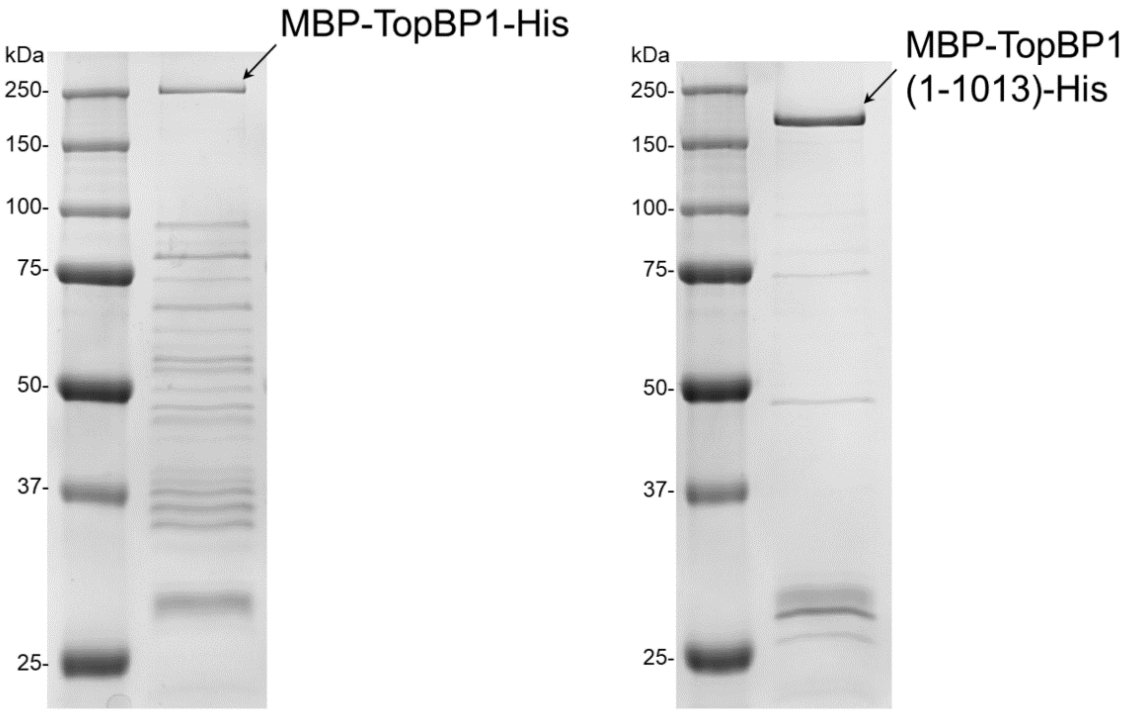

Supplementary Figure 1. Purified TopBP1.
Purified proteins were separated by SDS-PAGE and stained by CBB.

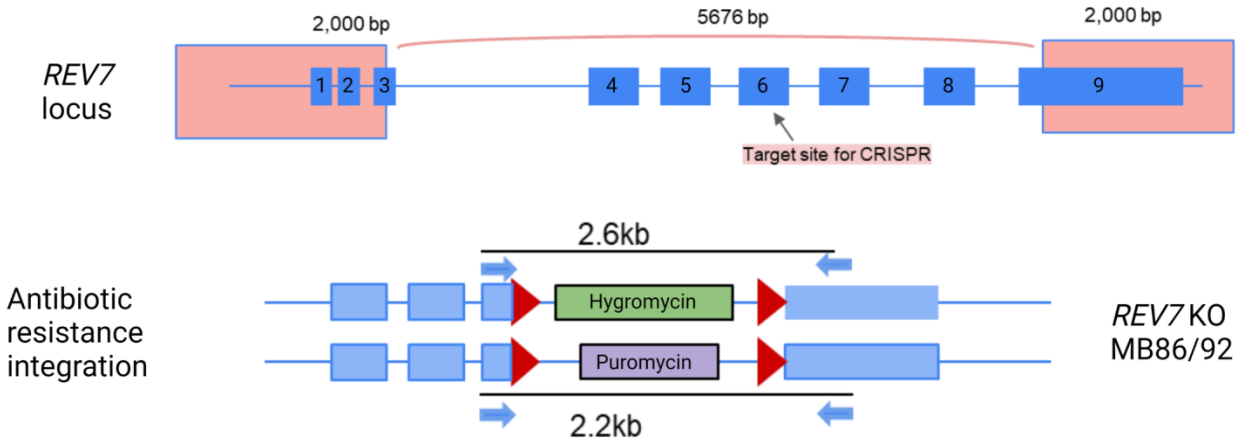

Supplementary Figure 2. ***REV7* KO cell line generation.**
Schematic of the *REV7* locus containing 9 exons. Pink boxes represent the arms of our expression vectors, and CRISPR gRNA target site indicated by the arrow. Below, schematic of Hygromycin and Puromycin resistance integration resulting in two *REV7* KO clones: MB86 and MB92.
Figure modified from Sara Nipper.

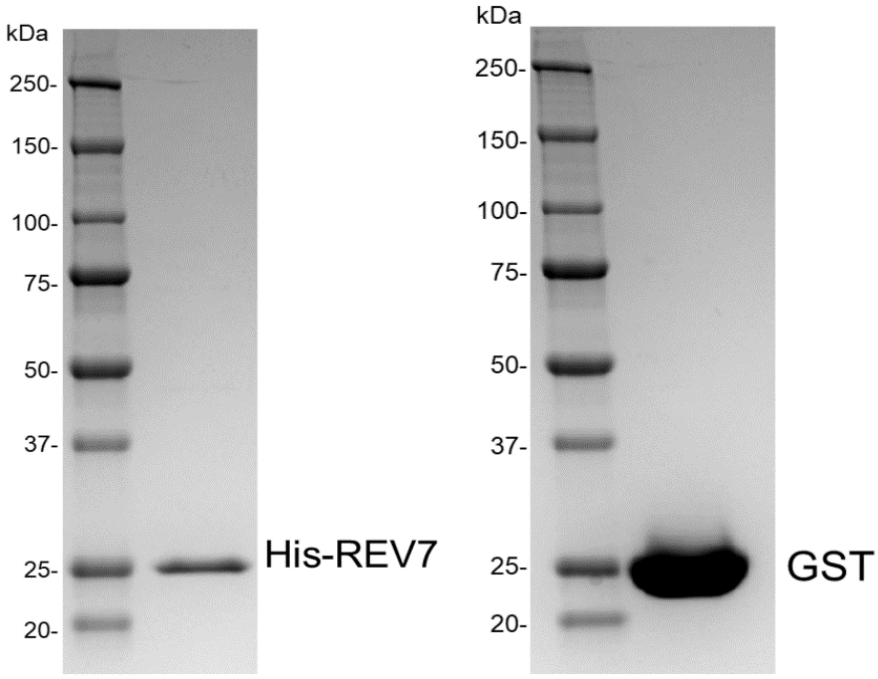

Supplementary Figure 3. Purified His-REV7 and GST for pulldown assays.
Purified proteins were separated by SDS-PAGE and stained by CBB.

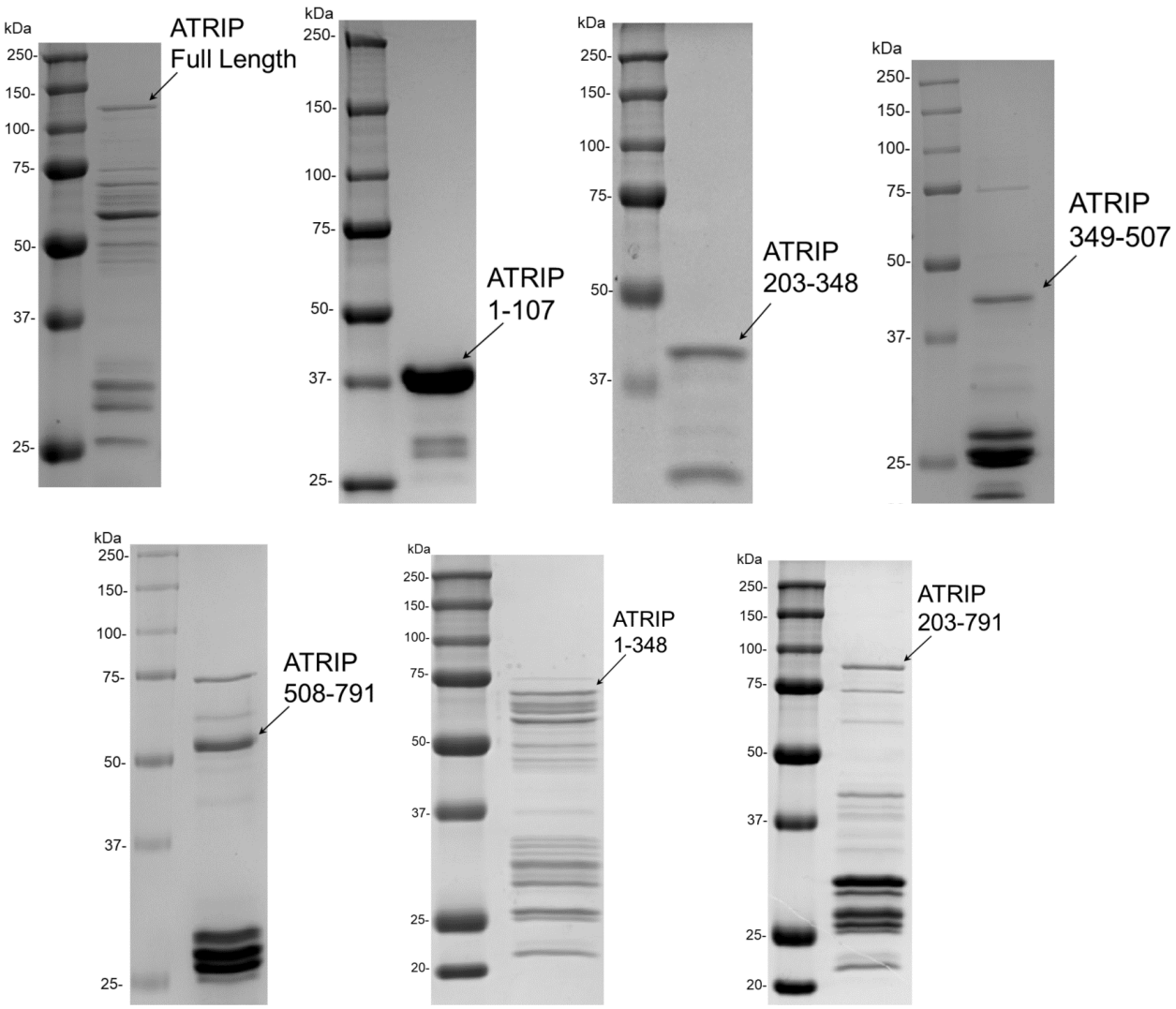

Supplementary Figure 4. Purified ATRIP fragments for pulldown assays.
Purified proteins were separated by SDS-PAGE and stained by CBB.

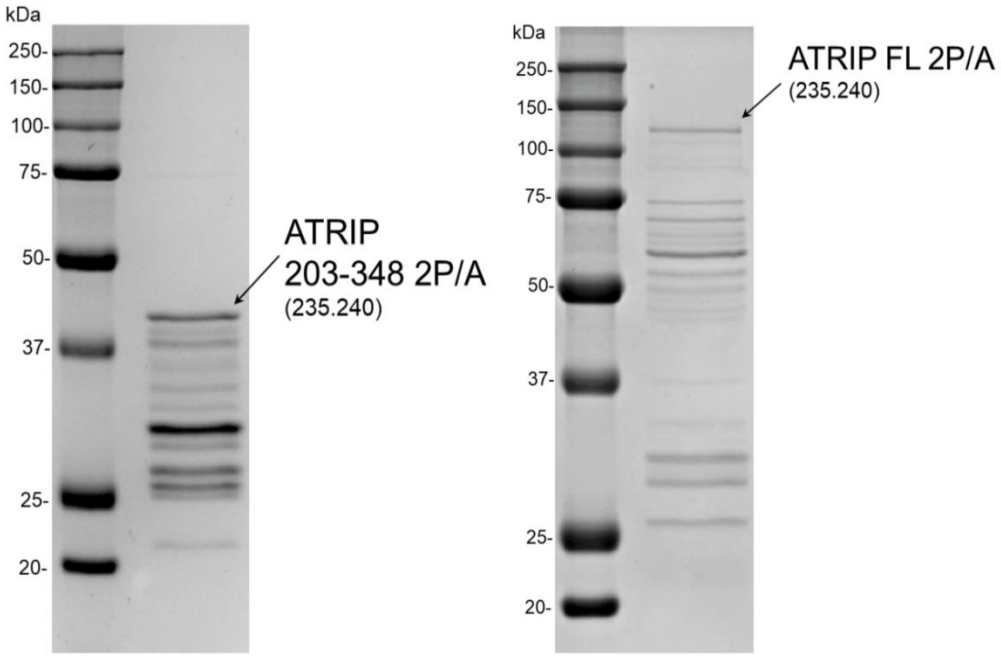

Supplementary Figure 5. Purified ATRIP 2P/A for Pulldown assays.
Purified proteins were separated by SDS-PAGE and stained by CBB.

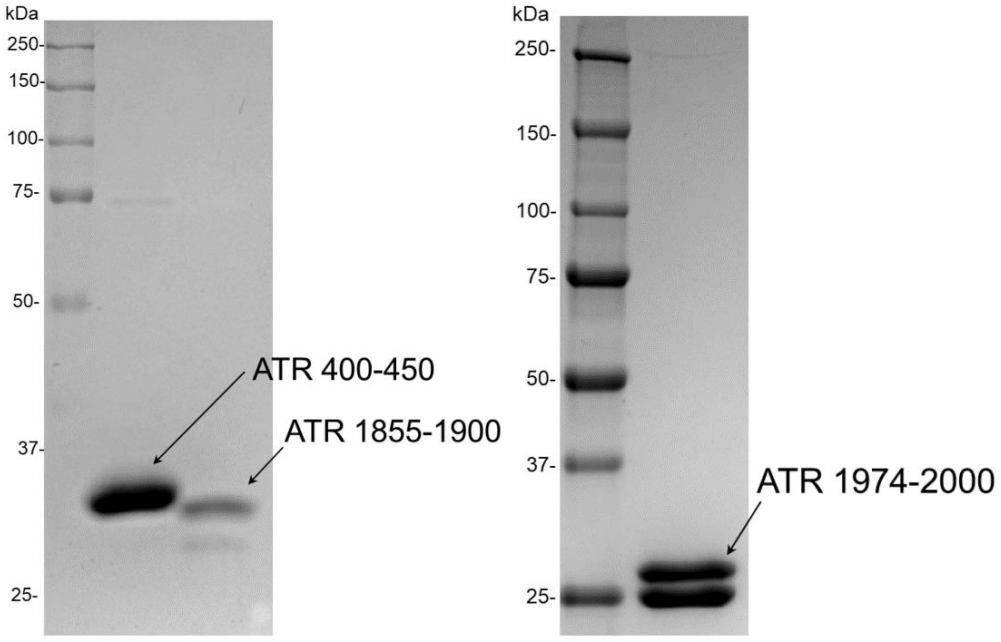

Supplementary Figure 6. Purified ATR fragments for pulldown assays.
Purified proteins were separated by SDS-PAGE and stained by CBB.

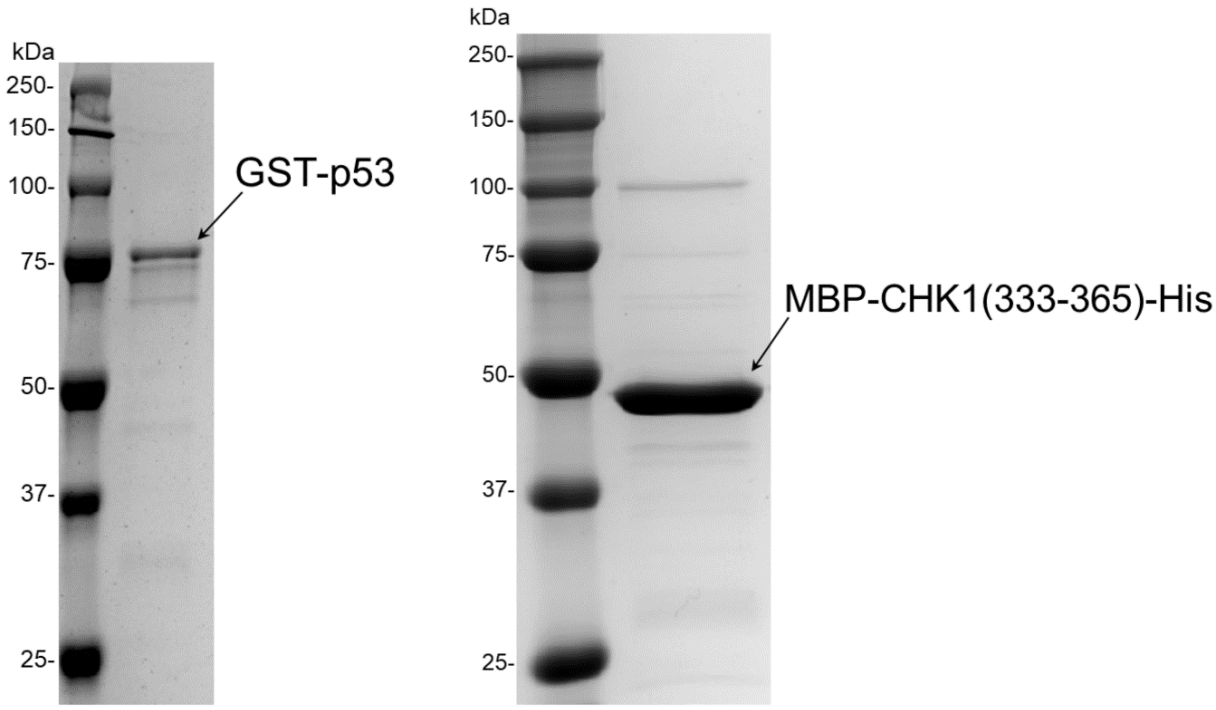

Supplementary Figure 7. Purified substrates for kinase assays.
Purified proteins were separated by SDS-PAGE and stained by CBB.

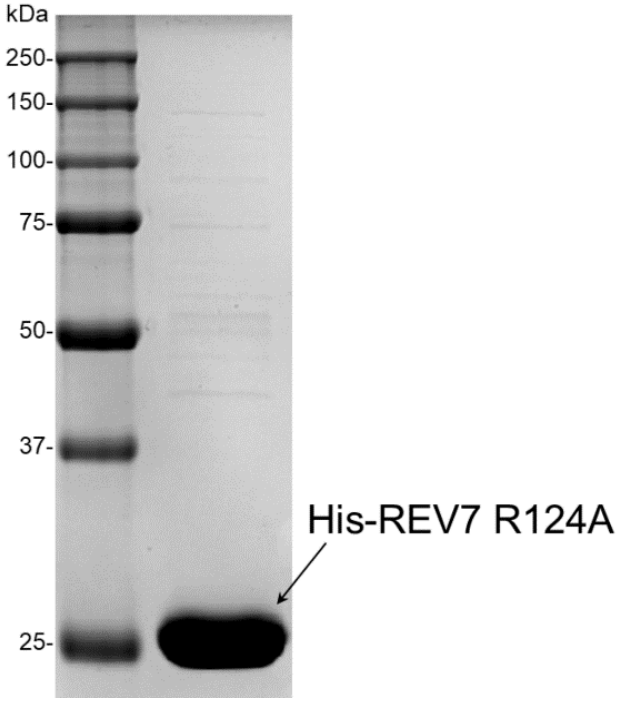

Supplementary Figure 8. Purified His-REV7 R124A for pulldown assay.
Purified proteins were separated by SDS-PAGE and stained by CBB.